



HAL
open science

The topological gradient method for semi-linear problems and application to edge detection and noise removal.

Audric Drogoul, Gilles Aubert

► **To cite this version:**

Audric Drogoul, Gilles Aubert. The topological gradient method for semi-linear problems and application to edge detection and noise removal.. Inverse Problems and Imaging , 2015, 10 (1). hal-01018200v3

HAL Id: hal-01018200

<https://hal.science/hal-01018200v3>

Submitted on 30 Oct 2015

HAL is a multi-disciplinary open access archive for the deposit and dissemination of scientific research documents, whether they are published or not. The documents may come from teaching and research institutions in France or abroad, or from public or private research centers.

L'archive ouverte pluridisciplinaire **HAL**, est destinée au dépôt et à la diffusion de documents scientifiques de niveau recherche, publiés ou non, émanant des établissements d'enseignement et de recherche français ou étrangers, des laboratoires publics ou privés.

The topological gradient method for semi-linear problems and application to edge detection and noise removal.

AUDRIC DROGOULAUDRIC.DROGOUL@INRIA.FR

audric.drogoul@inria.fr, Univ. Nice Sophia Antipolis, CNRS, LJAD, UMR 7351, 06100 Nice, France

GILLES AUBERT

gaubert@unice.fr, Univ. Nice Sophia Antipolis, CNRS, LJAD, UMR 7351, 06100 Nice, France

Mathematics Subject Classification— 35J30, 49Q10, 49Q12, 94A08, 94A13

Key words— Topological gradient, Semi-linear problem, Poisson noise, Speckle noise, Segmentation, Restoration

Abstract

The goal of this paper is to apply the topological gradient method to edge detection and noise removal for images degraded by various noises and blurs. First applied to edge detection for images degraded by a Gaussian noise, we propose here to extend the method to blurred images contaminated either by a multiplicative noise of gamma law or to blurred Poissonian images. We compute, both for perforated and cracked domains, the topological gradient for each noise model. Then we present an edge detection/restoration algorithm based on this notion and we apply it to the two degradation models previously described. We compare our method with other classical variational approaches such that the Mumford-Shah and TV restoration models and with the classical Canny edge detector. Some experimental results showing the efficiency, the robustness and the rapidity of the method are presented.

1 Introduction

An important problem in image analysis is the reconstruction of an original image u from an observed image f . In general this includes restoration and edge detection processes. The transformation between f and u originates from two phenomena. The first phenomenon is related to the acquisition process (blur created by a wrong lens ajustement or by a movement, Poissonian photons emission rates ...) and the second is due to the signal transmission. A lot of methods to reconstruct such degraded images exist: stochastic methods [23, 14], wavelets decomposition [32, 19], morphological methods [38]. Here we are interested with variational approaches [9]. In this context, the most famous model is the Mumford-Shah functional [34] but other works based on variational methods do exist [9]. Among more recent papers, we can cite [6] for restoration of images contaminated by speckle noise, [17] for blind restoration of Poissonian images, and [37] for an overview of image restoration degraded by different type of noise.

In this paper we tackle the edge detection problem by using the topological gradient method. First introduced for cracks detection by Sokolowski et al. [39] and Masmoudi [33], and applied in optimal design and mechanics ([3, 2, 5]), this notion consists in the study of the variations of a cost function $j(\Omega) = J(\Omega, u_\Omega)$

with respect to a topological variation, where $J(\Omega, u)$ is of the form $J(\Omega, u) = \int_{\Omega} F(u, \nabla u, \nabla^2 u, \dots)$ and u_{Ω} is a solution of a PDE defined on the image domain Ω . In order to compute the topological gradient, we remove from Ω a small object ω_{ε} of size $\varepsilon \rightarrow 0$ centered at a point $x_0 \in \Omega$ (generally a ball or a segment) and we set $\Omega_{\varepsilon} = \Omega \setminus \overline{\omega_{\varepsilon}}$. Two typical examples are: for small $\varepsilon > 0$ (a) $\Omega_{\varepsilon} = \Omega \setminus \{x_0 + \varepsilon B\}$ and (b) $\Omega_{\varepsilon} = \Omega \setminus \{x_0 + \varepsilon \sigma(\mathbf{n})\}$, where $B = B(O, 1)$ is the unit ball of \mathbb{R}^2 and $\sigma(\mathbf{n})$ is a straight segment with normal n (a crack). We compute $\mathcal{S}(x_0) = \lim_{\varepsilon \rightarrow 0} \frac{j(\Omega_{\varepsilon}) - j(\Omega)}{\rho(\varepsilon)}$ where $\rho(\varepsilon)$ is a non negative function such that $\rho(\varepsilon) \rightarrow 0$ if $\varepsilon \rightarrow 0$ (in our context, $\rho(\varepsilon) = \varepsilon^2$). $\mathcal{S}(x_0)$ is called the topological gradient at x_0 . It measures the energy contained by a perturbation centered at x_0 . The type of structure to be detected depends on the choice of the cost function $J(\Omega, u)$. Recently this notion has been used in image processing and to the best of our knowledge the first works in this direction are those by [26, 31, 15]. Then other imaging problems such as inpainting, classification, demosaicing, super resolution, have been adressed using a topological gradient approach [10, 16, 11, 13, 12, 29, 30]. In [15], only Gaussian additive noise is considered and in [30] blur has been introduced. In fact, in [30] more general degradations have been taken into account. The authors consider model of the form $f = Lu + b$ where f is the observed image, L a linear operator and b a Gaussian additive noise. They compute in the case of a crack the topological gradient and illustrate their approach for various imaging problems (edge detection/restoration, super resolution, demosaicing). Note also that topological gradient methods have been also applied for fine structures detection (e.g. points and filaments) [8, 7, 21]. In this case the cost function is based on second order derivatives. Edge detection/restoration in imaging are in general ill-posed inverse problems and one way to overcome this difficulty is to regularize them. A classical framework to do that is to use a Bayesian formulation which leads to the minimization of an energy consisting in two terms. The first one is a data fidelity term which takes into account both the statistic of the noise and the blur and the second one is an adequate regularizing term. For example if we suppose that the acquisition model is of the form $f = u + b$ where b is Gaussian noise then an anti-log-likelihood estimator amounts to choose as a data fidelity term the L^2 -norm $\|u - f\|_{L^2(\Omega)}^2$. If the noise follows another statistic, of course this term changes. The regularizing term is often based on an L^p norm of the gradient. Our main contribution is to generalize the results given in [30] to blurred images contaminated by Poissonian statistic and images degraded by speckle noise. We give the different expressions of the topological gradient associated to the cost function

$$J(\Omega, u) = \int_{\Omega} |\nabla u|^2 \quad (1)$$

and to equations of the following forms:

$$\text{(Speckle model)} \begin{cases} -\Delta u + K^* D_u \psi(x, Ku) = 0, & \text{in } \Omega \\ \partial_n u = 0, & \text{on } \partial\Omega \end{cases} \quad (2)$$

and

$$\text{(Poisson model)} \begin{cases} -\Delta u + \psi'_j \left(\int_{R_j^{N_0}} Ku \right) K^* \mathbb{1} = 0, & \text{in } R_j^{N_0} \\ \partial_n u = 0, & \text{on } \partial\Omega \text{ and } [u]_{\partial R_j^{N_0}} = 0 \quad \forall j \in \{1, \dots, N_0\} \end{cases} \quad (3)$$

where $R_j^{N_0}$ is a regular domain modeling pixel j , N_0 is the number of pixels and $[u]_{\partial R_j^{N_0}}$ denotes the jump of u across $\partial R_j^{N_0}$. We suppose that Ω is the disjoint union of $(R_j^{N_0})_{j \in \{1, \dots, N_0\}}$. The operator

$$K : L^2(\Omega) \longrightarrow L^2(\Omega)$$

is a convolution (generally positive and such that $K\mathbb{1} \neq 0$) representing the blur. We denote by K^* its adjoint. The functions $\psi(x, u)$ and $\psi_j(v)$ will be specified in section 4 and section 5.

Note that problems (2) and (3) are semi-linear and one of our contribution is to show they are well-posed and verify some maximum principles. Speckle noise is a multiplicative noise of gamma law, which is present in SAR images, laser images, microscope images [28, 25, 40]. A Poisson statistic occurs in confocal microscopy [20], emission tomography [41] and single-photon emission computed tomography [24].

In section 2, we recall the classical rationale justifying the modelization of the data fidelity term in a Bayesian approach. In section 3 we set the variational problem taking into account the blur. In section 4 we show that problem (2) is well-posed and give the associated topological gradient both for perforated and cracked domains (in fact, we study a more general class of problem (2)). In section 5 we treat the Poissonian model (3) whose energy is not standard. We summarize in Table 1 (section 6) all the expressions of the topological gradient according to the type of noise and to the infinitesimal perturbation. In section 7 we show how to apply the notion of topological gradient to restore degraded images. Finally in section 8, we present for all the models, the way to numerically implement the computation of the topological gradient and we display various experimental results illustrating each of them. We conclude this section by giving some notations and assumptions.

Notations and assumptions:

- $\Omega \subset \mathbb{R}^2$ is the image domain.
- $\|u\|_{0,\Omega}$ the $L^2(\Omega)$ -norm.
- $H^1(\Omega) = \{u \in L^2(\Omega) \mid \nabla u \in L^2(\Omega)\}$ the Sobolev space endowed with the norm $\|u\|_{1,\Omega}^2 = \|u\|_{L^2(\Omega)}^2 + \|\nabla u\|_{L^2(\Omega)}^2$.
- $|u|_{1,\Omega} = \|\nabla u\|_{L^2(\Omega)}$ the semi-norm on $H^1(\Omega)$.
- $\|u\|_{H^1(\Omega)/\mathbb{R}}$ the norm on the quotient space $H^1(\Omega)/\mathbb{R}$.
- $B_r(x)$ the ball centered at x and of radius r , B_r the ball centered at 0 and of radius r and $B = B_1$ denotes the unit ball.
- Ω_ε the perturbed domain defined by either (a) $\Omega_\varepsilon = \Omega \setminus \overline{\{x_0 + \varepsilon B\}}$ or (b) $\Omega_\varepsilon = \Omega \setminus \overline{\{x_0 + \varepsilon \sigma(\mathbf{n})\}}$ where $\sigma(\mathbf{n})$ is the straight segment of length 2 centered at 0 and of normal \mathbf{n} .
- $\Omega_0 = \Omega$
- $J_\varepsilon(u) = J(\Omega_\varepsilon, u)$.
- $f : \Omega \rightarrow \mathbb{R}$ is the observed image, $u : \Omega \rightarrow \mathbb{R}$ the image to be recovered.
- R_j^N models pixel j , where N is the number of pixels. We suppose that Ω is the disjoint union of the R_j 's.
- $f^N = (f_j^N)_{1 \leq j \leq N}$ (resp. $u^N = (u_j^N)_{1 \leq j \leq N}$) is a discrete version of f (resp. u) defined by $f_j^N = \frac{1}{|R_j^N|} \int_{R_j^N} f$ (resp. $u_j^N = \frac{1}{|R_j^N|} \int_{R_j^N} u$).

Only the proof for a perforated domain (a) is performed since for a cracked domain (b) the explicit dependency on the data is killed by the fact that the crack has a null Lebesgue measure.

2 A Bayesian approach

In this section we recall, in the discrete setting, the classical Bayesian approach allowing to deduce the suitable variational model for restoring noisy images. The reasoning is as follows: we express the a priori conditional probability $P(u^N = u | f^N = f)$ and then we look for u^N as the value maximizing $P(u^N = u | f^N = f)$ (a Maximum A Priori (MAP) estimator). Thanks to the Bayes rule, we have:

$$P(u^N = u | f^N = f) = \begin{cases} \frac{P(f^N = f | u^N = u)P(u^N = u)}{P(f^N = f)}, & \text{if } P(f^N = f) > 0 \\ 0, & \text{otherwise} \end{cases}$$

$P(f^N = f | u^N = u)$ depends on the noise model and $P(u^N = u)$ is an a priori density probability. Writing that u^N is a minimum of $-\log(P(u^N = u | f^N = f))$ leads to looking for u^N as the solution of

$$u^N = \underset{u \in \mathbb{R}^N}{\operatorname{argmin}} E^N(\Omega, u)$$

where

$$E^N(\Omega, u) = -\log(P(f^N = f | u^N = u)) - \log(P(u^N = u)) \quad (4)$$

The a priori density $P(u^N = u)$ plays the role of a regularizing term. In analogy to statistical mechanics, a priori densities are frequently Gibbs functions [23] of the form:

$$P(u^N = u) = C \times e^{-\frac{\gamma}{2} G^N(u)}, \quad \gamma > 0$$

where $G^N(u)$ is a discrete version of a non negative energy functional $G(u)$ and C is a constant. Here we will consider that $G^N(u) = J^N(\Omega, u)$ is a discretization of $J(\Omega, u)$ defined in (1). The choice of the density probability $P(f^N = f | u^N = u)$ depends on the statistic of the model to be considered. Below we review respectively speckle and Poisson models.

(i) Speckle model

For SAR images, the classical modeling is (see [40]): $f^N = s^N u^N$ where u^N is the reflectance of the scene (which is to be recovered) and s^N the speckle noise. Let us explicit the law of s^N . SAR images are constructed from $L \in \mathbb{N}$ observations $f^{k,N}$ with $1 \leq k \leq L$ and for each observations we have $f^{k,N} = h^{k,N} u^N$. Generally $h^{k,N}$ is a random variable which follows a negative exponential law with mean 1. Then, the observed image f^N is construct from this L observations as:

$$f^N = \frac{1}{L} \sum_{k=1}^L f^{k,N} = \left(\frac{1}{L} \sum_{k=1}^L h^{k,N} \right) u^N$$

We set $s^N = \frac{1}{L} \sum_{k=1}^L h^{k,N}$; s^N follows a gamma law with density $P(s^N = s) = \frac{L^L}{\Gamma(L)} s^{L-1} e^{-Ls} \mathbf{1}_{\{s \geq 0\}}$ with $\Gamma(L) = (L-1)!$ (the mean of s^N is 1 and its variance $\frac{1}{L}$). Standard computations lead to

$$P(f^N = f | u^N = u) = \frac{1}{u} P\left(s^N = \frac{f}{u}\right) \quad (5)$$

Classically, it is assumed that f^N and u^N are independently distributed. Hence the density of $f^N|u^N$ is the product of the densities $\left(f_j^N|u_j^N\right)_{1 \leq j \leq N}$. By applying the $-\log$ function we deduce that (4) in this case rewrites as (up to a multiplicative constant)

$$E^N(\Omega, u) = \frac{L}{\gamma} \sum_{j=1}^N \left(\frac{f_j^N}{u_j} + \log(u_j) \right) + \frac{1}{2} J^N(\Omega, u) + C$$

for $u \in \mathbb{R}^N$ and $u > 0$, where C denotes a constant independent of u . The factor L can be neglected since it can be scaled with the constant γ . Passing to the limit as $N \rightarrow \infty$, we deduce the following continuous energy

$$E(\Omega, u) = \int_{\Omega} \frac{1}{\gamma} \left(\frac{f}{u} + \log(u) \right) dx + \frac{1}{2} J(\Omega, u) \quad (6)$$

(ii) *Speckle with log of the image (Speckle-log model)*

One drawback of (6) is that the data fidelity term is nonconvex. By setting, $v^N = \log(u^N)$ and $g^N = \log(f^N)$, we can still use the Bayesian reasoning with $v^N = g^N + \log(s^N)$. The expression of the data fidelity term is changed and taking the same Gibbs function ($G^N(v) = J^N(\Omega, v)$) we deduce the continuous energy:

$$E(\Omega, v) = \int_{\Omega} \frac{1}{\gamma} \left(v + e^{-(v-g)} \right) + \frac{1}{2} J(\Omega, v) \quad (7)$$

which is now a convex function of v . The recovered image is then $u = e^v$.

(iii) *Poissonian model*

This model is classical in astronomical and confocal microscopy imaging [20]. Poissonian statistic is due to the stochastic nature of photons counts at sensors. We set $N = N_0$ the number of sensors which are modelled by the $R_j^{N_0}$'s. To simplify notation, since N_0 is fixed we drop the superscript N_0 in all variables and we assume that $|R_j| = 1 \forall j \in \{1, \dots, N_0\}$. We assume that f is a piecewise constant function equal to f_j on each R_j . The observed image f_j is a realization of a Poisson statistic of mean and variance equal to $\lambda_j = \int_{R_j} u(x) dx$ where $x \mapsto u(x)$ is the continuous image to be recovered. Thanks to the independence of f_j and λ_j , the conditional probability $P(f|\lambda)$ is given by:

$$P(f|\lambda) = \prod_{j=1}^{N_0} \frac{\lambda_j^{f_j} e^{-\lambda_j}}{f_j!}$$

and by applying the $-\log$ function, we have:

$$-\log(P(f|\lambda)) = \sum_{j=1}^{N_0} \lambda_j - f_j \log(\lambda_j) + C$$

where C is a constant independent of u . We deduce the energy:

$$E(\Omega, u) = \frac{1}{\gamma} \sum_{j=1}^{N_0} \left(\int_{R_j} u(x) dx - f_j \log \left(\int_{R_j} u(x) dx \right) \right) + \frac{1}{2} J(\Omega, u) \quad (8)$$

3 Blurring modelling

In most imaging applications the optical material, the motion of the camera or of the target introduce a blur on the observed image (see [36]). Generally spatially invariant, the blur is modelled as a positive convolution operator $u \mapsto Ku$ with $K\mathbf{1} \neq 0$. We denote by K^N the $N \times N$ matrix associated to a discrete version of K on Ω . From section 2 we can deduce the following models adapted to each kind of noise and taking into account the blur:

1. Speckle model: the observed discrete image writes as $f^N = s^N K^N u^N$ and the energy is

$$E(\Omega, u) = \int_{\Omega} \frac{1}{\gamma} \left(\log(Ku) + \frac{f}{Ku} \right) + \frac{1}{2} J(\Omega, u) \quad (9)$$

2. Speckle-log model. We recall that the model writes as $g^N = v^N + \log(s^N)$ with $v^N = \log(K^N u^N)$. The deblurring cannot be handled simultaneously with the denoising process since in general the equation $v^N = \log(K^N u^N)$ is not invertible. In this case, it is then preferable to use (9).
3. Poissonian model: the observed image f_j is a realization of a Poissonian statistic of mean $\int_{R_j} Ku^N(x) dx$, so the energy is

$$E(\Omega, u) = \frac{1}{\gamma} \sum_{j=1}^{N_0} \left(\int_{R_j} Ku(x) dx - f_j \log \left(\int_{R_j} Ku(x) dx \right) \right) + \frac{1}{2} J(\Omega, u) \quad (10)$$

4 Speckle multiplicative noise

In this section we show that equation (2) admits a unique solution for a more general class of functions ψ including the speckle-log model. For that we consider the minimization problem:

$$\min_{u \in H^1(\Omega)} E(\Omega, u) := \int_{\Omega} \psi(x, Ku) + \frac{1}{2} J(\Omega, u) \quad (11)$$

4.1 Well-posedness of problem (2)

We begin by stating the hypotheses defining the class of functions $\psi(x, u)$ that we consider, including the speckle-log model (11).

Hypotheses 1. Let I be an interval of \mathbb{R} and $\psi : \Omega \times I \rightarrow \mathbb{R}$ such that

- (i) $u \mapsto \psi(x, u) \in C^3(I) \forall x \in \bar{\Omega}$
- (ii) $x \mapsto D_u \psi(x, u) \in C^0(\Omega) \forall u \in I$
- (iii) $\text{Inf}_{\bar{\Omega} \times \mathcal{W}} D_u^2 \psi(x, u) > 0$ for each compact \mathcal{W} of I .

(iv) ψ is bounded from below on $\Omega \times I$

(v) $\exists a, b \in I$ such that for all x , $D_u \psi(x, a) \leq 0$ and $D_u \psi(x, b) \geq 0$ with $[a, b] \subset I$.

Lemma 4.1. *Let $\psi(x, u)$ a function verifying Hypotheses 1, we assume that K is non decreasing and that $K\mathbb{1} \neq 0$, then (11) admits a unique solution $u_\Omega \in H^1(\Omega)$. Moreover, we have $\frac{a}{K\mathbb{1}} \leq u_\Omega \leq \frac{b}{K\mathbb{1}}$.*

Proof. To shorten notations, when it is not ambiguous, we denote $\psi(u)$ for $\psi(x, u)$.

Existence: Let (u_n) a minimizing sequence. There exists a constant C_1 such that $E(\Omega, u_n) \leq C_1$. As $\psi(x, u)$ is bounded from below on $\Omega \times I$ there exists a constant C_2 such that $\int_\Omega \psi(x, u_n) \geq C_2$. Therefore:

$$\int_\Omega |\nabla u_n|^2 \leq \max(C_1, C_1 - C_2)$$

Let be $a' = \frac{a}{K\mathbb{1}}$ (s.t. $Ka' = a$), $v_n = \max(u_n, a')$ and $\Omega_n^- = \Omega \cap \{u_n \leq a'\}$, we have $v_n \geq a'$ and

$$E(\Omega, v_n) - E(\Omega, u_n) = - \int_{\Omega_n^-} |\nabla u_n|^2 + \int_{\Omega_n^-} \psi(a) - \psi(Ku_n)$$

By convexity $\psi(Ku_n) - \psi(Ka') \geq D_u \psi(a)(Ku_n - Ka')$, and from Hypothesis 1-(v) and using that K is not decreasing we get $\int_{\Omega_n^-} \psi(a) - \psi(Ku_n) \leq 0$. We deduce that $E(\Omega, v_n) \leq E(\Omega, u_n)$. Thus v_n is still a minimizing sequence and $v_n \geq a'$. Similarly by setting $b' = \frac{b}{K\mathbb{1}}$ and $w_n = \min(v_n, b')$, we get $w_n \leq b'$ and w_n is a minimizing sequence. Therefore we can suppose that any minimizing sequence u_n verifies $a' \leq u_n \leq b'$.

Thus u_n is bounded in $H^1(\Omega)$ and up to a subsequence there exists $u \in H^1(\Omega)$ such that $u_n \xrightarrow{L^2(\Omega)} u$ and $u_n \xrightarrow{H^1(\Omega)} u$ (where $\xrightarrow{H^1(\Omega)}$ stands for the weak topology). By using the lower semi-continuity of $J(\Omega, u)$ and Fatou's Lemma we obtain that u is a solution of (11). Moreover we have $a' \leq u \leq b'$ a.e. on Ω .

Uniqueness: From the existence, we can work on the set $\mathcal{H}(\Omega) = \{v \in H^1(\Omega), a' \leq v \leq b'\}$. Since $\psi(u)$ is strictly convex on $[a, b] \subset I$ and $J(\Omega, u)$ is strictly convex on $H^1(\Omega)$, we deduce that $E(\Omega, u)$ is strictly convex on $\mathcal{H}(\Omega)$ and admits a unique minimum. □

Since problem (11) and equation (2) are equivalent we deduce:

Corollary 1. *Under the same hypotheses as in Lemma 4.1, (2) admits a unique solution $u_\Omega \in H^1(\Omega)$. Moreover, we have $\frac{a}{K\mathbb{1}} \leq u_\Omega \leq \frac{b}{K\mathbb{1}}$.*

We apply below Lemma 4.1 to the speckle-log model for $K = I$.

Proposition 1. *Let f be such that $\exists \alpha, \beta \in \mathbb{R} \mid 0 < \alpha \leq f \leq \beta$. We assume that $K = I$, and $\psi(x, u) = u + e^{-(u-g(x))}$ where $g = \log(f)$. Then problem (11) has a unique solution $u \in H^1(\Omega)$. Moreover we have $\log(\alpha) \leq u \leq \log(\beta)$.*

Proof. A standard computation leads to $D_u \psi(u) = 1 - e^{-(u-g)}$ and $D_u^2 \psi(u) = e^{-(u-g)} > 0$. Hence $\psi(u)$ is strictly convex on \mathbb{R} . By using that $0 < \alpha \leq f \leq \beta$, we get

$$1 - e^{-(u-\log(\beta))} \leq D_u \psi(u) \leq 1 - e^{-(u-\log(\alpha))}$$

Let $a = \log(\alpha)$ and $b = \log(\beta)$, the following inequalities hold

$$D_u \psi(b) \geq 0 \text{ and } D_u \psi(a) \leq 0$$

From Lemma 4.1, there exists a unique function $u \in H^1(\Omega)$ solution of (11). Moreover we have $a \leq u \leq b$. □

In the next subsection we give the topological gradients for perforated and cracked domains when $K = I$ and ψ satisfying Hypotheses 1.

4.2 Computation of the topological gradient for a perforated domain

For a perforated domain $\Omega_\varepsilon = \Omega \setminus \overline{\{x_0 + \varepsilon B\}}$, let u_ε be the solution of the problem

$$(\mathcal{P}_\varepsilon) \begin{cases} -\Delta u_\varepsilon + D_u \psi(x, u_\varepsilon) = 0 & \text{in } \Omega_\varepsilon \\ \partial_n u_\varepsilon = 0 & \text{on } \partial \Omega_\varepsilon \end{cases} \quad (12)$$

By setting $\tilde{J}(\Omega, u) = -\int_\Omega D_u \psi(x, u) u$, from the variational formulation of the equation verified by u_ε , computing the topological gradient associated to $J(\Omega, u)$ is equivalent to compute the one associated to $\tilde{J}(\Omega, u)$. To give the topological gradient expression we need (see [2, 22, 39]) to introduce an adjoint solution v_ε defined by

$$(\mathcal{Q}_\varepsilon) \begin{cases} -\Delta v_\varepsilon + D_u^2 \psi(x, u_0) v_\varepsilon = -\partial \tilde{J}(u_0) = D_u \psi(x, u_0) + D_u^2 \psi(x, u_0) u_0 & \text{in } \Omega_\varepsilon \\ \partial_n v_\varepsilon = 0 & \text{on } \partial \Omega_\varepsilon \end{cases} \quad (13)$$

where u_0 denotes the solution of (12) for $\varepsilon = 0$ and $\partial \tilde{J}(u_0)$ the gradient of $\tilde{J}(\Omega, \cdot)$ at u_0 .

Theorem 4.2. *Let ψ satisfying Hypotheses 1, then the topological gradient I_{Lap}^b associated to problem (12) with the cost function $J_\varepsilon(u) = \int_{\Omega_\varepsilon} |\nabla u|^2$ for a perforated domain is*

$$I_{Lap}^b(x_0) = -2\pi \nabla u_0(x_0) \cdot \nabla v_0(x_0) + \pi D_u \psi(x_0, u_0) (u_0(x_0) - v_0(x_0)) \quad (14)$$

with u_0 and v_0 respectively solution (12) and (13) for $\varepsilon = 0$.

Proof. The proof of Theorem 4.2 is given in [27, 22] under slightly different assumptions; see also [22]. \square

Remark 1. *The adjoint problem (13) is linear and we can notice that the strict convexity of $u \mapsto \psi(x, u)$ is necessary to $(\mathcal{Q}_\varepsilon)$ be coercive. Since $u \mapsto \psi(x, u)$ is $C^2(I)$ and thanks to Lemma 4.1 there exist two constants $A, B \in \mathbb{R}$ such that $\forall x \in \Omega$*

$$A \leq D_u \psi(x, u_0) + D_u^2 \psi(x, u_0) u_0(x) \leq B$$

Hence (13) is well-posed. Moreover, we have the following inequality

$$\frac{A}{\sup_\Omega D_u^2 \psi(x, u_0)} \leq v_\varepsilon \leq \frac{B}{\inf_\Omega D_u^2 \psi(x, u_0)}$$

4.3 Expression of the topological gradient for a cracked domain

For the cracked domain $\Omega_\varepsilon = \Omega \setminus \overline{\{x_0 + \varepsilon \sigma(\mathbf{n})\}}$ the data fidelity term does not affect the topological gradient expression since the crack has a $2d$ Lebesgue measure equal to 0. The asymptotic expansion of u_ε and v_ε are similar and the computation of the topological gradient is the same as in the linear case and is given in [5, 22].

Theorem 4.3. *The topological gradient I_{Lap}^c associated to problem (12) and to the cost function $J_\varepsilon(u) = \int_{\Omega_\varepsilon} |\nabla u|^2$ for a cracked domain is*

$$I_{Lap}^c(x_0) = \min_{\|\mathbf{n}\|=1} \mathcal{I}(x_0, \mathbf{n}) \quad (15)$$

with $\mathcal{I}(x_0, \mathbf{n}) = -\pi \nabla u_0(x_0) \cdot \mathbf{n} \nabla v_0(x_0) \cdot \mathbf{n}$

with u_0 and v_0 respectively solution of (12) and (13) for $\varepsilon = 0$.

5 Poissonian model with blurring

In this section we consider the Poissonian model (3) whose associated energy is given by:

$$\min_{u \in H^1(\Omega)} E(\Omega, u) := \sum_{j=1}^{N_0} \psi_j \left(\int_{R_j} Ku \right) + \frac{1}{2} J(\Omega, u) \quad (16)$$

with $\psi_j(x) = \frac{1}{\gamma} (x - f_j \log(x))$. First we show that problem (16) is well-posed, then we compute the topological gradient for a perforated domain and we give the expression for a cracked domain.

5.1 Well-posedness of problem (16)

Proposition 2. *We assume that $0 < f_j < +\infty \ \forall j \in \{1, \dots, N_0\}$ and $K\mathbb{1} \neq 0$, then problem (16) with $\psi_j(x) = x - f_j \log(x)$ for $j \in \{1, \dots, N_0\}$ admits a unique solution $u \in H^1(\Omega)$.*

Moreover this solution verifies $\alpha \leq \int_{R_j} Ku \leq \beta, \forall j \in \{1, \dots, N_0\}$ with $\alpha = \frac{\min_j f_j}{N}$ and $\beta = \int_{\Omega} f = \sum_{j=1}^{N_0} f_j$.

Proof. Existence: We must add a priori to (16) the condition $\int_{R_i} Ku > 0, \forall i \in \{1, \dots, N_0\}$, thus let us define the space $\mathcal{H}(\Omega) = \left\{ u \in H^1(\Omega) \mid \int_{R_i} Ku > 0 \ \forall i \in \{1, \dots, N_0\} \right\}$. Then problem (16) rewrites as:

$$\min_{u \in \mathcal{H}(\Omega)} \frac{1}{2} \int_{\Omega} |\nabla u|^2 + \sum_j \psi_j \left(\int_{R_j} Ku \right)$$

Let $(u_n)_n$ a minimizing sequence of $E(\Omega, u)$ in $\mathcal{H}(\Omega)$. There exists a constant $D > 0$ such that $E(\Omega, u_n) \leq D$. If $C = \sum_j \min_{x \in]0, +\infty[} \psi_j(x) = \sum_j f_j - f_j \log(f_j) > -\infty$, then:

$$0 \leq \int_{\Omega} |\nabla u_n|^2 \leq 2 \max(D, D - C)$$

Since $\int_{\Omega} |\nabla u_n|^2 \geq 0$, we have $\sum_j \psi_j \left(\int_{R_j} Ku_n \right) \leq D$. Setting $\mathcal{K}_i = \sum_{j \neq i} \min_x \psi_j$, it is straightforward that $\psi_i \left(\int_{R_i} Ku_n \right) \leq D - \mathcal{K}_i$ and then

$$0 < \underline{E}_i \leq \int_{R_i} Ku_n \leq \bar{E}_i \quad (17)$$

with $\bar{E}_i = \max \{ \psi_i^{-1}(D - \mathcal{K}_i) \}$ and $\underline{E}_i = \min \{ \psi_i^{-1}(D - \mathcal{K}_i) \}$ (we recall the notation $\psi_i^{-1}(b) = \{x \in]0, \infty[\text{ s.t. } \psi_i(x) = b\}$). Hence the constraint $\int_{R_i} Ku_n > 0$ is fulfilled. We deduce that $\sum_i \underline{E}_i \leq \int_{\Omega} Ku_n = \sum_i \int_{R_i} Ku_n \leq \sum_i \bar{E}_i$. Then we write u_n as $u_n = v_n + w_n$ where $w_n = \frac{1}{|\Omega|} \int_{\Omega} u_n$. Since $\nabla v_n = \nabla u_n$ and $\int_{\Omega} v_n = 0$, from Poincaré-Wirtinger, there exists $F \geq 0$ such that $\|v_n\|_{L^2(\Omega)} \leq F$. Moreover, we have

$$\left| \int_{\Omega} Kw_n \right| = |K\mathbb{1}| \left| \int_{\Omega} Ku_n \right| \leq \left| \int_{\Omega} Kv_n \right| + \left| \int_{\Omega} Ku_n \right| \leq \|K\|_{L^2(\Omega)} F + \sum_i \bar{E}_i$$

Thus, since $K\mathbb{1} \neq 0$, we get that $\int_{\Omega} u_n$ is bounded and thus u_n is bounded in $L^2(\Omega)$. So, there exist a sub-sequence u_{n_k} (still denoted u_n) and $u \in H^1(\Omega)$ such that $u_n \xrightarrow{L^2(\Omega)} u$ and $u_n \xrightarrow{H^1(\Omega)} u$. We deduce that $\int_{\Omega} |\nabla u|^2 \leq \liminf \int_{\Omega} |\nabla u_n|^2$ and $\int_{R_i} Ku_n \rightarrow \int_{R_i} Ku$. By continuity, we have $\psi_i \left(\int_{R_i} Ku_n \right) \rightarrow \psi_i \left(\int_{R_i} Ku \right) \forall i \in \{1, \dots, N_0\}$ and

$$E(\Omega, u) \leq \liminf E(\Omega, u_n)$$

which proves that u is a minimizer of $E(\Omega, u)$.

Bounds: If u is the solution of (16) then $D_u E(\Omega, u) \cdot v = 0 \quad \forall v \in H^1(\Omega)$ i.e.

$$\int_{\Omega} \nabla u \cdot \nabla v + \sum_{j=1}^{N_0} \psi'_j \left(\int_{R_j} Ku \right) \int_{R_j} Kv = 0, \quad \forall v \in H^1(\Omega) \quad (18)$$

with $\psi'_j \left(\int_{R_j} Ku \right) = 1 - \frac{f_j}{\int_{R_j} Ku}$.

(i) By taking $v = 1$, we get the equality $N_0 = \sum_j \frac{f_j}{\int_{R_j} Ku}$. As $\frac{f_j}{\int_{R_j} Ku} \geq 0, \forall j \in \{1, \dots, N_0\}$ and if $i_0 = \operatorname{argmin}_i \int_{R_i} Ku$, we have $N_0 \geq \frac{f_{i_0}}{\int_{R_{i_0}} Ku}$ which leads to $\int_{R_{i_0}} Ku \geq \frac{f_{i_0}}{N_0} \geq \frac{\min_i f_i}{N_0} > 0$.

(ii) By taking $v = u$, we obtain the inequality $\sum_i \int_{R_i} Ku - f_i \leq 0$ which leads to $\max_i \int_{R_i} Ku \leq \sum_i \int_{R_i} Ku \leq \sum_i f_i$.

Uniqueness: From the two previous bounds we can minimize $E(\Omega, u)$ over the convex set

$\mathcal{V}_{\alpha}^{\beta}(\Omega) = \left\{ u \in H^1(\Omega), \alpha \leq \int_{R_j} Ku \leq \beta \right\}$. Since $\psi_j(s)$ is strictly convex on $[\alpha, \beta]$ for all $j \in \{1, \dots, N_0\}$, we get that $u \mapsto \psi_j \left(\int_{R_j} Ku \right)$ is strictly convex on $H(\Omega)$. As $|u|_{1, \Omega}^2$ is strictly convex, $E(\Omega, \cdot)$ is strictly convex on $\mathcal{V}_{\alpha}^{\beta}(\Omega)$ and then $E(\Omega, \cdot)$ has a unique minimum. \square

Since problem (16) and equation (3) are equivalent, we deduce:

Corollary 2. *Under the same hypotheses as in Proposition 2, equation (3) admits a unique solution $u_{\Omega} \in H^1(\Omega)$. Moreover, we have $\alpha \leq \int_{R_j} Ku \leq \beta, \forall j \in \{1, \dots, N_0\}$ with $\alpha = \frac{\min_j f_j}{N_0}$ and $\beta = \int_{\Omega} f = \sum_{j=1}^{N_0} f_j$.*

Remark 2.

We can show that Proposition 2 holds as soon as ψ_j is bounded from below for $j \in \{1, \dots, N_0\}$ and strictly convex on $I \subset \mathbb{R}$. In the general case α and β are implicitly defined in function of ψ_j .

5.2 Computation of the topological gradient for a perforated domain

We suppose that $x_0 \in \Omega \setminus \cup_j \partial R_j$ and for ε sufficiently small we set j_0 the index such that $R_{j_0} \supset B_{\varepsilon}(x_0)$. For $j \in \{1, \dots, N_0\}$, let R_j^{ε} be the domain equal to $R_{j_0} \setminus \overline{B_{\varepsilon}(x_0)}$ if $j = j_0$ and R_j otherwise. Finally, let u_{ε} be the unique solution of problem (3) replacing Ω by Ω_{ε} :

$$(\mathcal{P}_{\varepsilon}) \begin{cases} -\Delta u_{\varepsilon} + \psi'_j(I_j^{\varepsilon}(Ku_{\varepsilon})) K^* \mathbf{1} = 0, & \text{in } R_j^{\varepsilon} \\ \partial_n u_{\varepsilon} = 0 \text{ on } \partial \Omega_{\varepsilon} & \text{and} \quad [u_{\varepsilon}]_{\partial R_j} = 0 \end{cases} \quad (19)$$

where $I_j^{\varepsilon}(u) = \int_{R_j^{\varepsilon}} u$. As for the speckle-log model, by setting $\tilde{J}(\Omega, u) = -\sum_{j=1}^{N_0} \psi'_j(I_j(Ku)) I_j(Ku)$, from the variational formulation of the equation verified by u_{ε} , computing the topological gradient associated to $J(\Omega, u)$ is equivalent to compute the one associated to $\tilde{J}(\Omega, u)$. To compute the topological gradient we need to introduce an adjoint solution v_{ε} defined by:

$$\begin{cases} -\Delta v_{\varepsilon} + \psi''_j(I_j(Ku_0)) I_j^{\varepsilon}(Kv_{\varepsilon}) K^* \mathbf{1} = -\partial \tilde{J}_j(u_0) = K^* \mathbf{1} & \text{in } R_j^{\varepsilon} \\ \partial_n v_{\varepsilon} = 0 \text{ on } \partial \Omega_{\varepsilon} & \text{and} \quad [v_{\varepsilon}]_{\partial R_j} = 0 \end{cases} \quad (20)$$

where $I_j(u) = \int_{R_j} u$ and $\partial \tilde{J}_j(u_0)$ denotes the gradient of $\tilde{J}_j(u) = -\psi'_j(I_j(Ku))I_j(Ku)$ at u_0 .

We now give the main result of this section.

Theorem 5.1. *The topological gradient I_{Lap}^b associated to problem (19) and to the cost function $J_\varepsilon(u) = \int_{\Omega_\varepsilon} |\nabla u|^2$ for a perforated domain is*

$$\begin{aligned} I_{Lap}^b(x_0) &= -2\pi \nabla u_0(x_0) \cdot \nabla v_0(x_0) + \pi \psi'_{j_0}(I_{j_0}(Ku_0))(Ku_0(x_0) - Kv_0(x_0)) \\ &\quad + \pi \psi''_{j_0}(I_{j_0}(Ku_0))Ku_0(x_0)(I_{j_0}(Ku_0) - I_{j_0}(Kv_0)) \end{aligned} \quad (21)$$

with u_0 and v_0 are respectively solution of (19) and (20) for $\varepsilon = 0$.

Proof. We split the proof in three steps and we assume without loss of generality that $x_0 = 0$.

Step 1 This step is dedicated to the computation of the difference $J_\varepsilon(u_\varepsilon) - J_0(u_0)$. Using the variational formulation of u_ε : find $u_\varepsilon \in H^1(\Omega_\varepsilon)$ s.t.

$$A_\varepsilon(u_\varepsilon, v) := \int_{\Omega_\varepsilon} \nabla u_\varepsilon \cdot \nabla v + \sum_{j=1}^{N_0} \int_{R_j^\varepsilon} \psi'_j(I_j^\varepsilon(Ku_\varepsilon))Kv = 0 \quad \forall v \in H^1(\Omega_\varepsilon) \quad (22)$$

we have $J_\varepsilon(u_\varepsilon) = \tilde{J}_\varepsilon(u_\varepsilon)$ with:

$$\tilde{J}_\varepsilon(u) = - \sum_{j=1}^{N_0} \int_{R_j^\varepsilon} \psi'_j(I_j^\varepsilon(Ku))Ku = - \sum_{j=1}^{N_0} \psi'_j(I_j^\varepsilon(Ku))I_j^\varepsilon(Ku)$$

By denoting $\phi_j(s) = \psi'_j(s)s$, the difference $J_\varepsilon(u_\varepsilon) - J_0(u_0)$ writes

$$J_\varepsilon(u_\varepsilon) - J_0(u_0) = \tilde{J}_\varepsilon(u_\varepsilon) - \tilde{J}_\varepsilon(u_0) = - \sum_{j=1}^{N_0} \phi_j(I_j^\varepsilon(Ku_\varepsilon)) - \phi_j(I_j(Ku_0))$$

Using a Taylor expansion of $\phi_j(s)$ at $I_j(Ku_0)$ and by remarking that $I_j^\varepsilon(Ku_\varepsilon) - I_j(Ku_0)$ rewrites $I_j^\varepsilon(K(u_\varepsilon - u_0))$ when $j \neq j_0$ and $I_j^\varepsilon(K(u_\varepsilon - u_0)) - \int_{B_\varepsilon} Ku_0$ when $j = j_0$, we have:

$$J_\varepsilon(u_\varepsilon) - J_0(u_0) = L_\varepsilon(u_\varepsilon - u_0) + \mathcal{M}_\varepsilon + \mathcal{E}_1 \quad (23)$$

with

$$\begin{aligned} L_\varepsilon(u) &= - \sum_{j=1}^{N_0} \phi'_j(I_j(Ku_0))I_j^\varepsilon(Ku) \quad \mathcal{M}_\varepsilon = \phi'_{j_0}(I_{j_0}(Ku_0)) \int_{B_\varepsilon} Ku_0 \\ \mathcal{E}_1 &= - \sum_{j=1}^{N_0} \phi''_j(\eta_\varepsilon^j)I_j^\varepsilon(K(u_\varepsilon - u_0))^2 \end{aligned} \quad (24)$$

where $\eta_\varepsilon^j \in]I_j(Ku_0), I_j^\varepsilon(Ku_\varepsilon)[\subset]\alpha, \beta]$.

Step 2. In this step we introduce the adjoint problem in order to estimate the linear term $L_\varepsilon(u_\varepsilon - u_0)$ in (23). For that we need to linearize (22) w.r.t u . A Taylor expansion gives:

$$\psi'_j(I_j^\varepsilon(Ku_\varepsilon)) - \psi'_j(I_j(Ku_0)) = \psi''_j(I_j(Ku_0))(I_j^\varepsilon(Ku_\varepsilon) - I_j(Ku_0)) + \frac{1}{2} \psi_j^{(3)}(\xi_\varepsilon^j)(I_j^\varepsilon(Ku_\varepsilon) - I_j(Ku_0))^2$$

with $\xi_\varepsilon^j \in]I_j(Ku_0), I_j^\varepsilon(Ku_\varepsilon)[\subset [\alpha, \beta]$. As a consequence we have

$$A_\varepsilon(u_\varepsilon, v) = \widetilde{A}_\varepsilon(u_0, v) + b_\varepsilon(u_\varepsilon - u_0, v) + c_\varepsilon(v) + d_\varepsilon(v) \quad (25)$$

with

$$\begin{aligned} \widetilde{A}_\varepsilon(u, v) &= \int_{\Omega_\varepsilon} \nabla u \cdot \nabla v + \sum_{j=1}^{N_0} \psi_j'(I_j(Ku)) \int_{R_j^\varepsilon} K v \\ b_\varepsilon(u, v) &= \int_{\Omega_\varepsilon} \nabla u \cdot \nabla v + \sum_{j=1}^{N_0} \psi_j''(I_j(Ku_0)) I_j^\varepsilon(Ku) \int_{R_j^\varepsilon} K v \\ c_\varepsilon(v) &= \frac{1}{2} \sum_{j=1}^{N_0} \psi_j^{(3)}(\xi_\varepsilon^j) (I_j^\varepsilon(Ku_\varepsilon) - I_j(Ku_0))^2 \int_{R_j^\varepsilon} K v \\ d_\varepsilon(v) &= -\psi_{j_0}''(I_{j_0}(Ku_0)) \int_{B_\varepsilon} Ku_0 \int_{R_{j_0}^\varepsilon} K v \end{aligned}$$

Let us introduce now the adjoint problem:

$$\text{find } v_\varepsilon \in H^1(\Omega_\varepsilon) \text{ s.t. } b_\varepsilon(u, v_\varepsilon) = -L_\varepsilon(u) \quad \forall u \in H^1(\Omega_\varepsilon) \quad (26)$$

It is easily seen that (26) is the variational formulation of (20). From (23) and (25), we obtain

$$\begin{aligned} J_\varepsilon(u_\varepsilon) - J_0(u_0) &= L_\varepsilon(u_\varepsilon - u_0) + \mathcal{M}_\varepsilon + \mathcal{E}_1 = -b_\varepsilon(u_\varepsilon - u_0, v_\varepsilon) + \mathcal{M}_\varepsilon + \mathcal{E}_1 \\ &= -A_\varepsilon(u_\varepsilon, v_\varepsilon) + \widetilde{A}_\varepsilon(u_0, v_\varepsilon) + c_\varepsilon(v_\varepsilon) + d_\varepsilon(v_\varepsilon) + \mathcal{M}_\varepsilon + \mathcal{E}_1 \\ &= \widetilde{A}_\varepsilon(u_0, v_\varepsilon) + \mathcal{E}_2 + \mathcal{N}_\varepsilon + \mathcal{M}_\varepsilon + \mathcal{E}_1 \end{aligned} \quad (27)$$

with

$$\mathcal{E}_2 = c_\varepsilon(v_\varepsilon) \quad \text{and} \quad \mathcal{N}_\varepsilon = d_\varepsilon(v_\varepsilon) \quad (28)$$

By using an integration by parts and equation (19) for $\varepsilon = 0$, $\widetilde{A}_\varepsilon(u_0, v_\varepsilon)$ expresses as

$$\begin{aligned} \widetilde{A}_\varepsilon(u_0, v_\varepsilon) &= - \int_{\partial B_\varepsilon} \partial_n u_0 v_\varepsilon - \int_{\Omega_\varepsilon} \Delta u_0 v_\varepsilon + \sum_{j=1}^{N_0} \psi_j'(I_j(Ku_0)) \int_{R_j^\varepsilon} v_\varepsilon \\ &= - \int_{\partial B_\varepsilon} \partial_n u_0 v_\varepsilon \end{aligned}$$

In the sequel, we need to extend v_ε inside the ball B_ε . To do that, for $\varphi \in H^{1/2}(\partial B_\varepsilon)$, we denote by l_ε^φ the harmonic function defined by

$$\begin{cases} \Delta l_\varepsilon^\varphi = 0 \text{ in } B_\varepsilon \\ l_\varepsilon^\varphi = \varphi \text{ on } \partial B_\varepsilon \end{cases}$$

For $v \in H^1(\Omega_\varepsilon)$ we set $l_\varepsilon^{v_\varepsilon} = l_\varepsilon^{v_\varepsilon|_{\partial B_\varepsilon}}$. By integration by parts, $\widetilde{A}_\varepsilon$ rewrites

$$\begin{aligned} \widetilde{A}_\varepsilon(u_0, v_\varepsilon) &= - \int_{\partial B_\varepsilon} \partial_n u_0 l_\varepsilon^{v_\varepsilon} = - \int_{\partial B_\varepsilon} \partial_n u_0 (l_\varepsilon^{w_\varepsilon} + v_0) \\ &= - \int_{B_\varepsilon} (\Delta u_0 (l_\varepsilon^{w_\varepsilon} + v_0) + \nabla \tilde{u}_0 \cdot \nabla (l_\varepsilon^{w_\varepsilon} + v_0)) \\ &= - \int_{B_\varepsilon} \Delta u_0 (l_\varepsilon^{w_\varepsilon} + v_0) - \int_{\partial B_\varepsilon} \tilde{u}_0 \partial_n (l_\varepsilon^{w_\varepsilon} + v_0) + \int_{B_\varepsilon} \tilde{u}_0 \Delta (l_\varepsilon^{w_\varepsilon} + v_0) \\ &= - \int_{B_\varepsilon} \psi_{j_0}'(I_{j_0}(Ku_0)) \left(\int_{B_\varepsilon} K l_\varepsilon^{w_\varepsilon} + \int_{B_\varepsilon} K v_0 \right) - \int_{\partial B_\varepsilon} \tilde{u}_0 (\partial_n l_\varepsilon^{w_\varepsilon} + \partial_n v_0) + \int_{B_\varepsilon} \tilde{u}_0 \Delta v_0 \\ &= \mathcal{H}_\varepsilon + \mathcal{L}_\varepsilon + \mathcal{E}_3 + \mathcal{E}_4 \end{aligned}$$

with $\tilde{u}_0 = u_0 - u_0(0)$, $w_\varepsilon = v_\varepsilon - v_0$ and

$$\begin{aligned}\mathcal{H}_\varepsilon &= - \int_{\partial B_\varepsilon} \tilde{u}_0 (\partial_n v_0 + \partial_n l_\varepsilon^{w_\varepsilon}) \quad , \quad \mathcal{L}_\varepsilon = - \psi'_{j_0} (I_{j_0}(Ku_0)) \int_{B_\varepsilon} K v_0 \\ \mathcal{E}_3 &= \int_{B_\varepsilon} \tilde{u}_0 \Delta v_0 \quad , \quad \mathcal{E}_4 = - \psi'_{j_0} (I_{j_0}(Ku_0)) \int_{B_\varepsilon} K l_\varepsilon^{w_\varepsilon}\end{aligned}\tag{29}$$

Step 3. In this step we give the asymptotic expansion of all the previous terms.

Proposition 3. *Let \mathcal{M}_ε , \mathcal{N}_ε , \mathcal{H}_ε , \mathcal{L}_ε , \mathcal{E}_1 , \mathcal{E}_2 , \mathcal{E}_3 and \mathcal{E}_4 given by (24), (28) and (29), then we have the following estimations:*

$$\begin{aligned}J_\varepsilon(u_\varepsilon) - J_0(u_0) &= \mathcal{M}_\varepsilon + \mathcal{N}_\varepsilon + \mathcal{H}_\varepsilon + \mathcal{L}_\varepsilon + \sum_{i=1}^4 \mathcal{E}_i \\ \mathcal{M}_\varepsilon &= \pi \varepsilon^2 (\psi'_{j_0} (I_{j_0}(Ku_0)) + \psi''_{j_0} (I_{j_0}(u_0)) I_{j_0}(Ku_0)) Ku_0(0) + o(\varepsilon^2) \\ \mathcal{N}_\varepsilon &= -\pi \varepsilon^2 \psi''_{j_0} (I_{j_0}(Ku_0)) Ku_0(0) I_{j_0}(Kv_0) + o(\varepsilon^2) \\ \mathcal{H}_\varepsilon &= -2\pi \varepsilon^2 \nabla u_0(0) \cdot \nabla v_0(0) + o(\varepsilon^2) \\ \mathcal{L}_\varepsilon &= -\pi \varepsilon^2 \psi'_{j_0} (I_{j_0}(Ku_0)) Kv_0(0) + o(\varepsilon^2)\end{aligned}\tag{30}$$

and $\mathcal{E}_i \sim o(\varepsilon^2)$ for $i \in \llbracket 1..3 \rrbracket$.

Proof. The first equality is straightforward. A Taylor expansion of u_0 at 0 gives the first estimation. Again a Taylor expansion of u_0 at 0, Lemma 9.4 (see Appendix A) and the fact that $R_{j_0}^\varepsilon \xrightarrow{\varepsilon \rightarrow 0} R_{j_0}$ give the second estimation. For \mathcal{H}_ε , from Lemmas 9.1 and 9.4 we have:

$$\begin{aligned}\mathcal{H}_\varepsilon &= \int_{\partial B} (u_0 - u_0(0)) \left(\partial_n l_\varepsilon^{\varepsilon P(\frac{x}{\varepsilon})} + \partial_n v_0 \right) + \int_{\partial B_\varepsilon} (u_0 - u_0(0)) \partial_n l_\varepsilon^{e_\varepsilon} \\ &= \varepsilon^2 \nabla u_0(0) \cdot \int_{\partial B} \lambda(x) x + \mathcal{F}_1 + \mathcal{F}_2\end{aligned}$$

with

$$\begin{aligned}\lambda(x) &= -2 \nabla v_0(0) \cdot \mathbf{n} \\ \mathcal{F}_1 &= \int_{\partial B_\varepsilon} (u_0 - u_0(0)) (\partial_n v_0 - \nabla v_0(0) \cdot \mathbf{n}) = O(\varepsilon^3) \\ \mathcal{F}_2 &= \int_{\partial B_\varepsilon} (u_0 - u_0(0)) \partial_n l_\varepsilon^{e_\varepsilon} = O(\varepsilon^3 \sqrt{-\log(\varepsilon)})\end{aligned}$$

For \mathcal{F}_2 it suffices to make a change of variable and use the trace theorem on $B_2 \setminus \bar{B}$:

$$\begin{aligned}\|\partial_n l_\varepsilon^{e_\varepsilon}(\varepsilon X)\|_{-1/2, \partial B} &\leq \frac{1}{\varepsilon} |l_\varepsilon^{e_\varepsilon}(\varepsilon X)|_{1, B} = \frac{1}{\varepsilon} |l^{e_\varepsilon(\varepsilon X)}(X)|_{1, B} \\ &\leq \frac{C}{\varepsilon} \|e_\varepsilon(\varepsilon X)\|_{H^{1/2}(\partial B)/\mathbb{R}} \leq C \|e_\varepsilon(\varepsilon X)\|_{H^1(B_2 \setminus \bar{B})/\mathbb{R}}\end{aligned}$$

Now from the equivalence of the $H^1(B_2 \setminus \bar{B})/\mathbb{R}$ -norm with the semi-norm and a change of variable, we get $\|\partial_n l_\varepsilon^{e_\varepsilon}(\varepsilon X)\|_{-1/2, \partial B} \leq C |e_\varepsilon|_{1, \Omega_\varepsilon}$. By using Lemma 9.4, we obtain $\mathcal{F}_2 = O(\varepsilon^3 \sqrt{-\log(\varepsilon)})$. For \mathcal{E}_1 and \mathcal{E}_2 , we use Lemma 9.3, the boundedness of $\int_{\Omega_\varepsilon} K v_\varepsilon$ independently from ε and the fact that η_ε and ξ_ε^j are in $] \alpha, \beta [$:

$$|\mathcal{E}_i| \leq C \left(\int_{R_\varepsilon^j} K(u_\varepsilon - u_0) \right)^2 = O(\varepsilon^4 \log(\varepsilon)) \text{ for } 1 \leq i \leq 2$$

By using that $\Delta v_0 = \psi''_{j_0}(I_{j_0}(Ku_0))I_{j_0}(Kv_0) - K\mathbb{1}$ and a Taylor expansion of u_0 at 0 we get $|\mathcal{E}_3| = O(\varepsilon^3)$.

For \mathcal{E}_4 , by using a change of variable, the continuity of $\varphi \mapsto I^\varphi$ from $H^{1/2}(\partial B)$ to $H^1(B)$, the trace theorem on $B_2 \setminus \bar{B}$, again a change of variable and Lemma 9.4 we obtain:

$$\begin{aligned} |\mathcal{E}_4| &\leq C\varepsilon^2 \|I_\varepsilon^{w_\varepsilon}(\varepsilon X)\|_{0,B} = C\varepsilon^2 \|I^{w_\varepsilon(\varepsilon X)}(X)\|_{0,B} \\ &\leq C\varepsilon^2 \|w_\varepsilon(\varepsilon X)\|_{1/2,\partial B} \leq C \|w_\varepsilon(\varepsilon X)\|_{1,B_2 \setminus \bar{B}} \\ &\leq C\varepsilon^2 \left(\frac{1}{\varepsilon} \|w_\varepsilon\|_{0,\Omega_\varepsilon} + |w_\varepsilon|_{1,\Omega_\varepsilon} \right) \leq C\varepsilon^3 \sqrt{-\log(\varepsilon)} \end{aligned}$$

□

From Proposition 3, we deduce the expression of the topological gradient at $x_0 = 0$. A simple change of the coordinates system gives the result at any point $x_0 \in \Omega$.

□

5.3 Expression of the topological gradient for a cracked domain

For a cracked domain the computations are similar. The data fidelity term does not affect the expression of topological gradient because the crack has a $2d$ Lebesgue measure equal to 0.

Theorem 5.2. *The topological gradient I_{Lap}^c associated to problem (19) and to the cost function $J_\varepsilon(u) = \int_{\Omega_\varepsilon} |\nabla u|^2$ for a cracked domain is*

$$\begin{aligned} I_{Lap}^c(x_0) &= \min_{|\mathbf{n}|=1} \mathcal{J}(x_0, \mathbf{n}) \\ \text{with } \mathcal{J}(x_0, \mathbf{n}) &= -\pi \nabla u_0(x_0) \cdot \mathbf{n} \nabla v_0(x_0) \cdot \mathbf{n} \end{aligned} \tag{31}$$

with u_0 and v_0 are solution of (19) and (20) for $\varepsilon = 0$.

Remark 3. *The topological gradient is the same in the general case of functions $\psi_j \in C^3(I)$, strictly convex on an interval I and bounded from below on I . Just in the right hand-side of (20), $K^*\mathbb{1}$ must be replaced by $\phi'_j(I_j(Ku_0))K^*\mathbb{1}$ with $\phi_j(s) = \psi'_j(s)s$.*

6 Summary table of the topological gradient expressions

We summarize in Table 1, all the expressions of the topological gradient according to the type of noise and to the infinitesimal perturbation.

	Ball	Crack
Speckle-log ($K = I$)	$-2\pi\nabla u_0(x_0) \cdot \nabla v_0(x_0) + \pi D_u \psi(x_0, u_0)(u_0(x_0) - v_0(x_0))$ with $\psi(x, u) = \frac{1}{\gamma}(u - \log(f(x)) + f(x)e^{-u})$	$-\pi\nabla u_0(x_0) \cdot \mathbf{n} \nabla v_0(x_0) \cdot \mathbf{n}$
Poisson ($K \neq I$)	$-2\pi\nabla u_0(x_0) \cdot \nabla v_0(x_0) + \pi \psi'_{j_0}(I_{j_0}(Ku_0))(Ku_0(x_0) - Kv_0(x_0))$ $+ \pi \psi''_{j_0}(I_{j_0}(Ku_0)) Ku_0(x_0)(I_{j_0}(Ku_0) - I_{j_0}(Kv_0))$ with $\psi_{j_0}(x) = \frac{1}{\gamma}(x - f_{j_0} \log(x))$ and $I_{j_0}(v) = \int_{R_{j_0}} v$, where $R_{j_0} \ni x_0$	$-\pi\nabla u_0(x_0) \cdot \mathbf{n} \nabla v_0(x_0) \cdot \mathbf{n}$

Table 1: Summary of the topological gradient expressions

7 Restoration using the topological gradient for a cracked domain

As a by product the computation of the topological gradient I_{Lap}^c for a cracked domain allows to restore images degraded by blur or/and various noise statistics. Once I_{Lap}^c is computed, we define for a fixed threshold $\delta > 0$, the set $E_\delta = \{x \in \Omega; |I_{Lap}^c(x)| \geq \delta\}$ and the approximated characteristic function

$$\chi_\eta(x) = \begin{cases} \eta & \text{if } x \in E_\eta \\ 1 & \text{otherwise} \end{cases}$$

where η is a small positive parameter. Typically, we take $\eta = 10^{-5}$ in the numerical experiments. From the computation of I_{Lap}^c we also get the normalized direction $\tau = \mathbf{n}^\perp$ of the edge. If $\mathbf{n} = (\cos(\varphi), \sin(\varphi))$ is the normal to the crack given by I_{Lap}^c , we have $\vec{\tau} = (\sin(\varphi), -\cos(\varphi))$. Then, if f is the degraded observed image, we want to find a restored version $u \in H^1(\Omega)$ of f as the solution of the following anisotropic PDE:

$$\begin{cases} -\text{div}(P_\eta^\varphi(x) \nabla u) + K^* D_u \psi(x, Ku) = 0 & \text{in } \Omega \\ \partial_n u = 0 & \text{on } \Gamma \end{cases} \quad (32)$$

with

$$\psi(x, u) = \begin{cases} \frac{1}{\gamma} \sum_{j \in I_{ind}} \left(\int_{R_j} u - f_j \log \left(\int_{R_j} u \right) \right) \mathbb{1}_{R_j}(x) & \text{(Poisson model)} \\ \frac{1}{\gamma} \left(\log(u) + \frac{f(x)}{u} \right) & \text{(Speckle model)} \end{cases} \quad (33)$$

and where $P_\eta^\varphi(x)$ is a tensor constructed from $\varphi(x)$ and $\chi_\eta(x)$ and γ is a parameter to tune. More precisely, we choose $P_\eta^\varphi(x) \nabla u(x) = (\nabla u \cdot \tau) \tau + \chi_\eta(x) (\nabla u \cdot \mathbf{n}) \mathbf{n}$. A simple identification shows that $P_\eta^\varphi(x)$ is the matrix

$$P_\eta^\varphi(x) = \begin{pmatrix} n_2^2 + \chi_\eta(x) n_1^2 & n_1 n_2 (\chi_\eta(x) - 1) \\ n_1 n_2 (\chi_\eta(x) - 1) & n_1^2 + \chi_\eta(x) n_2^2 \end{pmatrix} \quad (34)$$

where $n_1 = \cos(\varphi(x))$ and $n_2 = \sin(\varphi(x))$. The interpretation of this matrix $P_\eta^\varphi(x)$ is as follows:

- (i) if x belongs to the background, thanks to the definition of $\chi_\eta(x)$, $P_\eta^\phi(x)$ writes as $P_\eta^\phi(x) = I$, so $\text{div}(P_\eta^\phi(x)\nabla u) = \Delta u$ and the smoothing is isotropic.
- (ii) if x belongs to an edge (i.e. $x \in E_\delta$), then $\chi_\eta(x)$ is close to zero and $P_\eta^\phi(x)\nabla u(x) \approx (\nabla u \cdot \tau)\tau$ and the diffusion is in the direction of the edge. As we will see in section 8 on numerical examples, the restoration results obtained when applying equation (32) are very good.

To compute a numerical solution of equation (32), we consider the associated strictly convex energy :

$$E(u) = \int_{\Omega} P_\eta^\phi \nabla u \cdot \nabla u + \langle \psi(x, u) \rangle$$

that we discretize by using a classical finite differences scheme. Then we compute the minimizer of the discrete energy by applying a Scale Gradient Projection (SGP) type algorithm described in Algorithm 2 below.

8 Numerical application to 2D imaging

In this section we illustrate the theory of the topological gradient by giving various experimental results for models (2) and (3).

The topological gradient expressions for the two models are stated in sections 4 and 5 and are summarized in section 6 (Table 1).

For each model, to compute the topological gradient (TG) we use Algorithm 1. The computation of the direct and adjoint solutions is specific to each model.

Algorithm 1 Computation of the topological gradient

- 1: Computation of u_0 and v_0 by using Algorithm 2 below.
 - 2: Computation of the derivatives of u_0 by convolution with derivative filters.
 - 3: Computation of the TG relatively to the model by using Table 1 and/or Theorems of section 4 and 5.
-

Remark 4. For a cracked domain, indicators I_{Lap}^c (15) and (31) are given by the minimal eigenvalue of a 2×2 symmetric matrix:

$$I_{Lap}^c = \lambda_{\min}(M_0)$$

with

$$M_0 = -\pi \frac{\nabla u_0 \nabla v_0^T + \nabla v_0 \nabla u_0^T}{2}$$

We first perform the discretization of problems (11) and (16) and then we give the experimental results. As the adjoint problems (13) and (20) are linear with non constant coefficients we discretize them by a finite difference scheme and we compute the discrete solution by using a sparse solver.

8.1 Solving numerically Poisson and Speckle-log models

In this section, we assume that f and u are vectors of \mathbb{R}^N and $\min f > 0$. By Proposition 1 and Proposition 2, problems (11) and (16) can be discretized as:

$$\text{(Speckle-log model)} \quad \min_{u \geq \log(\alpha_s)} J_S(u), \quad \alpha_s > 0 \quad (35a)$$

$$\text{(Poisson model)} \quad \min_{u \geq \alpha_p} J_p(u), \quad \alpha_p > 0 \quad (35b)$$

where $\alpha_s = \min f$ and $\alpha_p = \frac{\min f}{N}$; $J_p(u)$ and $J_s(u)$ are respectively the discrete versions of energies (10) and (7).

During the construction of a minimizing sequence $u^{(k)}$, the condition $u^{(k)} \geq \alpha_p$ for the Poisson model (respectively $u^{(k)} \geq \log(\alpha_s)$ for the speckle model) must be fulfilled at each step. Hence a projection ensures this condition. To solve these problems we use an iterative algorithm based on the SGP algorithm [18]. Let us write the discrete cost functions:

$$J_s(u) = -\frac{\gamma}{2} u^T A u + \sum_{i=1}^N \left(u_i - g_i + e^{-(u_i - g_i)} \right)$$

$$J_p(u) = -\frac{\gamma}{2} u^T A u + \sum_{i=1}^N (Ku)_i - f_i \log((Ku)_i)$$

where A is the Neumann Laplacian matrix, K is a discretization of the blurring operator (circulant block matrix if we assume that the image is periodic) and we recall that $g_i = \log(f_i)$. Let us give the main ideas of the SGP algorithm. The discrete energies J_s and J_p are denoted by J as soon as we do not use their expression and δ will be the number equal to α for the Poisson model and equal to $\log(\alpha)$ for the Speckle-log model. We set $\Lambda = \{u \in \mathbb{R}^N, u \geq \delta\}$. We want to find $u^* \in \Lambda$ such that $\nabla J(u^*) = 0$. At step k , a first order Taylor expansion at point $u = u^{(k)}$ leads to the following equation

$$\nabla J(u^{(k)}) + \nabla^2 J(u^{(k)})(u - u^{(k)}) = 0$$

If $\det(\nabla^2 J(u^{(k)})) \neq 0$, we get $u = u^{(k)} - \nabla^2 J(u^{(k)})^{-1} \nabla J(u^{(k)})$. We deduce by this reasoning that the direction of the descent algorithm can be given by $\nabla^2 J(u^{(k)})^{-1} \nabla J(u^{(k)})$, but the computation of this direction is very costly. We denote by \mathcal{D}_L the compact set of symmetric positive definite $N \times N$ matrices such that $\|D\| \leq L$ and $\|D^{-1}\| \leq \frac{1}{L}$. The main idea of the SGP algorithm is to construct two sequences α_k and $D_k \in \mathcal{D}_L$ such that $\alpha_k D_k$ approximates $\nabla^2 J(u^{(k)})$ and to project each iterate on Λ with respect to the norm $\|u\|_D = \sqrt{u^T D u}$. We set $P_{\Lambda, D^{-1}}$ for $D \in \mathcal{D}_L$ the projector on Λ with respect to the norm $\|\cdot\|_D$. For more details on Algorithm 2, we refer the reader to [18] and we only give some explanations on the construction of the sequences D_k and α_k . We choose $D_k = \text{diag}(d_i^k)$ with $d_i^k = \min\left(L, \max\left(\frac{1}{L}, \frac{\partial^2 J}{\partial u_i^2}(u^{(k)})^{-1}\right)\right)$. The approximation of the Hessian matrix $\nabla^2 J(u^{(k)})$ is $B(\alpha_k) = \alpha_k D_k$. By using a first order Taylor expansion of $\nabla J(u)$ at point $u^{(k-1)}$ we get that

$$\nabla J(u^{(k)}) - \nabla J(u^{(k-1)}) = \nabla^2 J(u^{(k)})(u^{(k)} - u^{(k-1)}) + o\left((u^{(k)} - u^{(k-1)})^2\right)$$

Hence two possible choices of α_k can be made:

$$\alpha_k^1 = \arg \min_{\alpha} \left\| B(\alpha_k) s^{(k-1)} - z^{(k-1)} \right\|_{D_k} = \frac{s^{(k-1)T} D_k^{-1} D_k^{-1} s^{(k-1)}}{s^{(k-1)T} D_k^{-1} z^{(k-1)}}$$

$$\alpha_k^2 = \arg \min_{\alpha} \left\| s^{(k-1)} - B(\alpha_k)^{-1} z^{(k-1)} \right\|_{D_k} = \frac{s^{(k-1)T} D_k z^{(k-1)}}{z^{(k-1)T} D_k D_k z^{(k-1)}}$$

where $s^{(k-1)} = u^{(k)} - u^{(k-1)}$ and $z^{(k-1)} = \nabla J(u^{(k)}) - \nabla J(u^{(k-1)})$. In [18] the choice of α_k is the output of an algorithm called SGP-SS Algorithm (SGP step length selection) which uses two thresholds $0 < \alpha_{\min} < \alpha_{\max}$.

Algorithm 2 SGP algorithm

```
1: Set  $u^{(0)} \geq \alpha$ ,  $\beta, \theta \in ]0, 1[$ ,  $0 < \alpha_{min} < \alpha_{max}$ ,  $L > 0$ , and fix a positive integer  $M$ .
2: for  $k = 0 : k_{max}$  do
3:   Choose the parameter  $\alpha_k \in [\alpha_{min}, \alpha_{max}]$  and the scaling matrix  $D_k \in \mathcal{D}_L$ 
4:   Projection:  $y^{(k)} \leftarrow P_{\Lambda, D_k^{-1}}(u^{(k)} - \alpha_k D_k \nabla f(u^{(k)}))$ 
5:   if  $y^{(k)} = u^{(k)}$  then
6:     Stop,  $u^{(k)}$  is a stationary point.
7:   end if
8:   Descent direction  $d^{(k)} = y^{(k)} - u^{(k)}$ ;
9:    $\lambda_k \leftarrow 1$  and  $J_{max} \leftarrow \max_{0 \leq j \leq \min(k, M-1)} J(u^{(k-j)})$ 
10:   $\lambda_k$  fixed by backtracking:
11:  while  $f(u^{(k)} + \lambda_k d^{(k)}) \leq J_{max} + \beta \lambda_k \nabla J(u^{(k)})^T d^{(k)}$  do
12:     $\lambda_k \leftarrow \theta \lambda_k$ 
13:  end while
14:   $u^{(k+1)} \leftarrow u^{(k)} + \lambda_k d^{(k)}$ 
15: end for
```

The derivative of the discrete cost functions J_p and J_s are:

$$\begin{aligned}\nabla J_p &= -\gamma A u - K^T \frac{f}{Ku} + K^T \mathbf{1} \\ \nabla^2 J_p &= -\gamma A + K^T \text{diag} \left(\frac{f}{(Ku)^2} \right) K \\ \nabla J_s &= -\gamma A u + 1 - e^{-(u-f)} \\ \nabla^2 J_s &= -\gamma A + \text{diag} \left(e^{-(u-f)} \right)\end{aligned}$$

where $\mathbf{1} \in \mathbb{R}^N$ denotes the vector whose each coordinate is equal to 1, $\text{diag}(x)$ for $x \in \mathbb{R}^N$ is the diagonal matrix with diagonal entries equal to x . For $x \in \mathbb{R}^N$ and $\varphi : \mathbb{R} \rightarrow \mathbb{R}$, $\varphi(x)$ stands for the vector $(\varphi(x_i))_{1 \leq i \leq N}$. The choice of the parameters in Algorithm 2 is the following: $\beta = 10^{-4}$, $\theta = 0.4$, $k_{max} = 600$, $M = 1$ and for the Poisson model (16) we set $\alpha_{min} = 10^{-10}$, $\alpha_{max} = 10^5$ while for the Speckle-log model (11) we set $\alpha_{min} = 10^{-5}$, $\alpha_{max} = 10^{15}$. The initial value of $u^{(0)}$ is either the observed image for the Poisson model or its logarithm for the Speckle-log model. Let us note that in the case of equation (32), the matrix A is the finite differences discretisation of the operator $\text{div}(P_\eta^\varphi \nabla \cdot)$ and for the speckle model of restoration we use the function $\psi(u) = \log(u) + \frac{f}{u}$.

8.2 Comparison of our method with some classical models

We compare the results given by the topological gradient approach with the ones performed by the Mumford-Shah and TV models. We will also compare our detection process with the well-known Canny edge detector.

Mumford-Shah model of segmentation/restoration and its approximation

Let u be the image of support Ω , the functional introduced by Mumford and Shah in 1989 (see [34]) is:

$$F(u, \gamma) = \int_{\Omega} |u - u_0|^2 + \lambda \int_{\Omega \setminus \bar{\gamma}} |\nabla u|^2 + \alpha \mathcal{H}^1(\gamma)$$

where f is the observed image, u is a function defined on $\Omega \setminus \bar{\gamma}$ (the restored version of f) and $\gamma \subset \Omega$ is the set of discontinuity of u . \mathcal{H}^1 is the Hausdorff measure of γ , λ and α are positive parameters. The difficulty is that the unknown are not of same nature: u is a function and γ is a set. Ambrosio and Tortorelli [1] proposed an approximation of this functional as follows:

$$\mathcal{F}_\varepsilon(u, b) = \int_{\Omega} \left[|u - f|^2 + \lambda b^2 |\nabla u|^2 + \alpha \left(\varepsilon |\nabla b|^2 + \frac{(b-1)^2}{4\varepsilon} \right) \right]$$

We will change the data fidelity term $|u - f|^2$ according to the a priori model (speckle and Poissonian models) i.e. we will compare (32) with the solution of (see [37]):

$$\min_{u \in H^1(\Omega), b \in H^1(\Omega)} \int_{\Omega} \left[\psi(x, Ku) + \lambda b^2 |\nabla u|^2 + \alpha \left(\varepsilon |\nabla b|^2 + \frac{(b-1)^2}{4\varepsilon} \right) \right] \quad (36)$$

where K is the blur operator, $u(x)$ is the restored image, $1 - b(x) \approx 0$ is the characteristic function of the edges and $\psi(x, u)$ is given in (33). We will call this model the Mumford-Shah model (MS).

TV model of restoration

The TV model is well-known: we search for a restored version u minimizing an energy functional which is the sum of the total variation $\|Du\|$ and a data fidelity term which depends on the a priori model (see [6] for the speckle model and [17] for the Poisson one). Thus, we will compare model (32) to:

$$\min_{u \in \mathcal{BV}(\Omega)} \int_{\Omega} |Du| + \lambda \psi(x, Ku) \quad (37)$$

where λ is a parameter, K the blur operator, and $\psi(u)$ is given in (33). In the sequel we call this model the TV model.

The Canny edge detector

We will also compare the edge detection performed by our approach with the Canny edge detector which is the norm of the gradient of a regularization of the image by a Gaussian convolution at scale σ . For more details on these models we refer the reader to [17, 6, 37, 34] and for the numerical approximations to [9] and the references therein.

For restoration comparisons on synthetic images we use two indicators:

- the PSNR which is defined for a noisy observation I of an image I_0 by

$$PSNR(I) = 10 \text{Log} \left(\frac{255^2}{\|I - I_0\|_2^2 / N} \right)$$

where N is the number of pixels in the image.

- the SSIM defined as

$$SSIM(I) = \frac{(2\mu_I \mu_{I_0} + c_1)(2cov(I, I_0) + c_2)}{(\mu_I^2 + \mu_{I_0}^2 + c_2)}$$

where μ_x stands for the mean of x , cov is the covariance operator and c_1 and c_2 are constants given for RGB images by $c_1 = (255k_1)^2$ and $c_2 = (255k_2)^2$ with $k_1 = 0.01$ and $k_2 = 0.03$.

8.3 Numerical results for the speckle-log model. Comparisons

In this section we illustrate the detection process given by I_{Lap}^c (15), I_{Lap}^b (14), $b(x)$ (computed with the MS model (36)) and the Canny edge detector. All edge detectors are displayed up to a normalisation in order to have edges in black and the background of the image in white. We also display the restoration performed by (32), the MS model (36) and the TV model (37).

On Fig. 1, we compare I_{Lap}^c (15) and I_{Lap}^b (14) for different values of γ with $b(x)$ and with the Canny edge detector for a synthetic speckled image. I_{Lap}^b seems more adapted to detect isotropic structures and we deduce that γ must be tuned with respect to the noise and to the size of structures to detect. Comparing I_{Lap}^c , MS and the Canny edge detector, similar results are obtained for the cheetah.

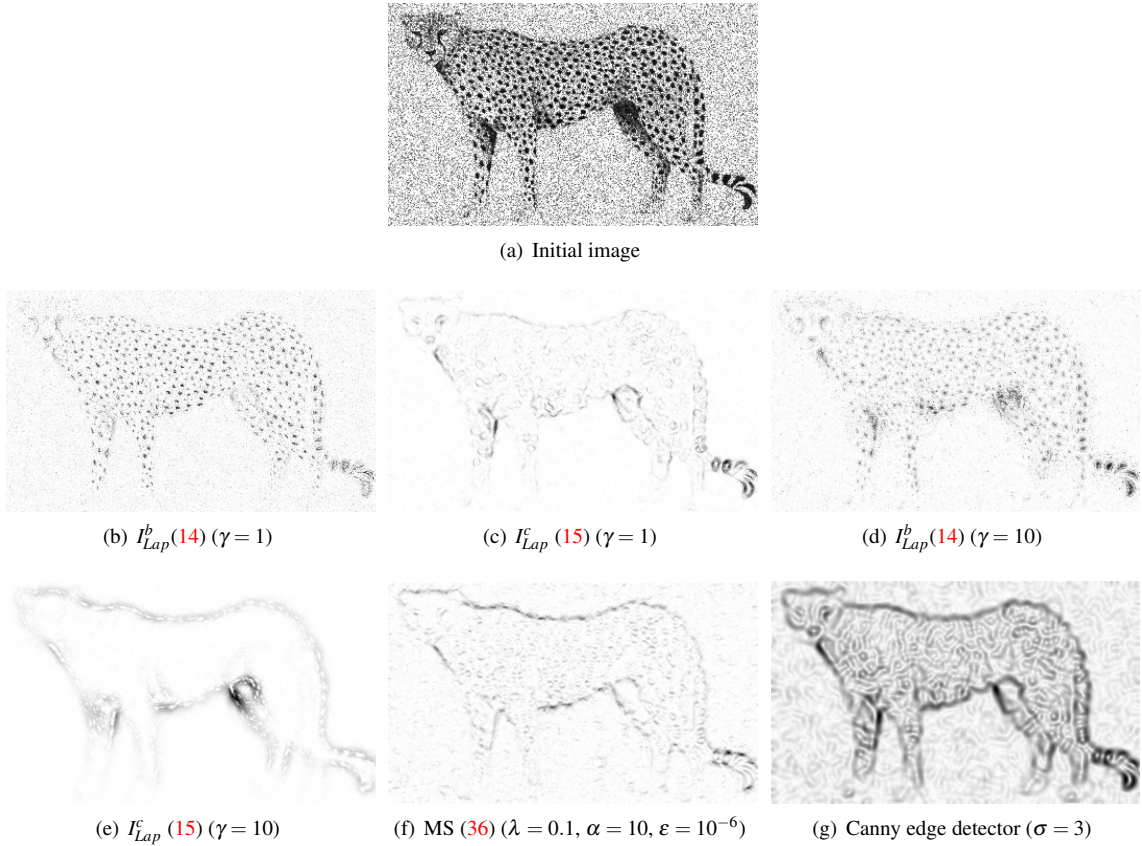


Figure 1: Comparison of (14) and (15) for different values of γ with the MS edge detection (36) and the Canny edge detector for an initial speckled image ($L = 6$) containing mainly isotropic small structures.

Remark 5. Let us note that for large γ an edge doubling phenomena appears for I_{Lap}^c on Fig. 1-(e). As shown in [4], in the linear case (Gaussian noise), the edge doubling can be avoided by using as cost function the opposite of the square of the L_2 -norm. More generally we have remarked that the edge doubling can be avoided for the speckle-log model by adding in the cost function the term $\int_{\Omega} \psi(u)$. Let us recall that the direct and adjoint models given in (12) and (13) are associated to the auxiliary cost function $\tilde{J}(\Omega, u) = -\int_{\Omega} D_u \psi(x, u) u$. Fig. 2 shows profiles of the direct and adjoint models and I_{Lap}^c (15) associated to $\tilde{J}(\Omega, u)$

and to $\tilde{J}_2(\Omega, u) = \tilde{J}(\Omega, u) + \int_{\Omega} \psi(u)$.

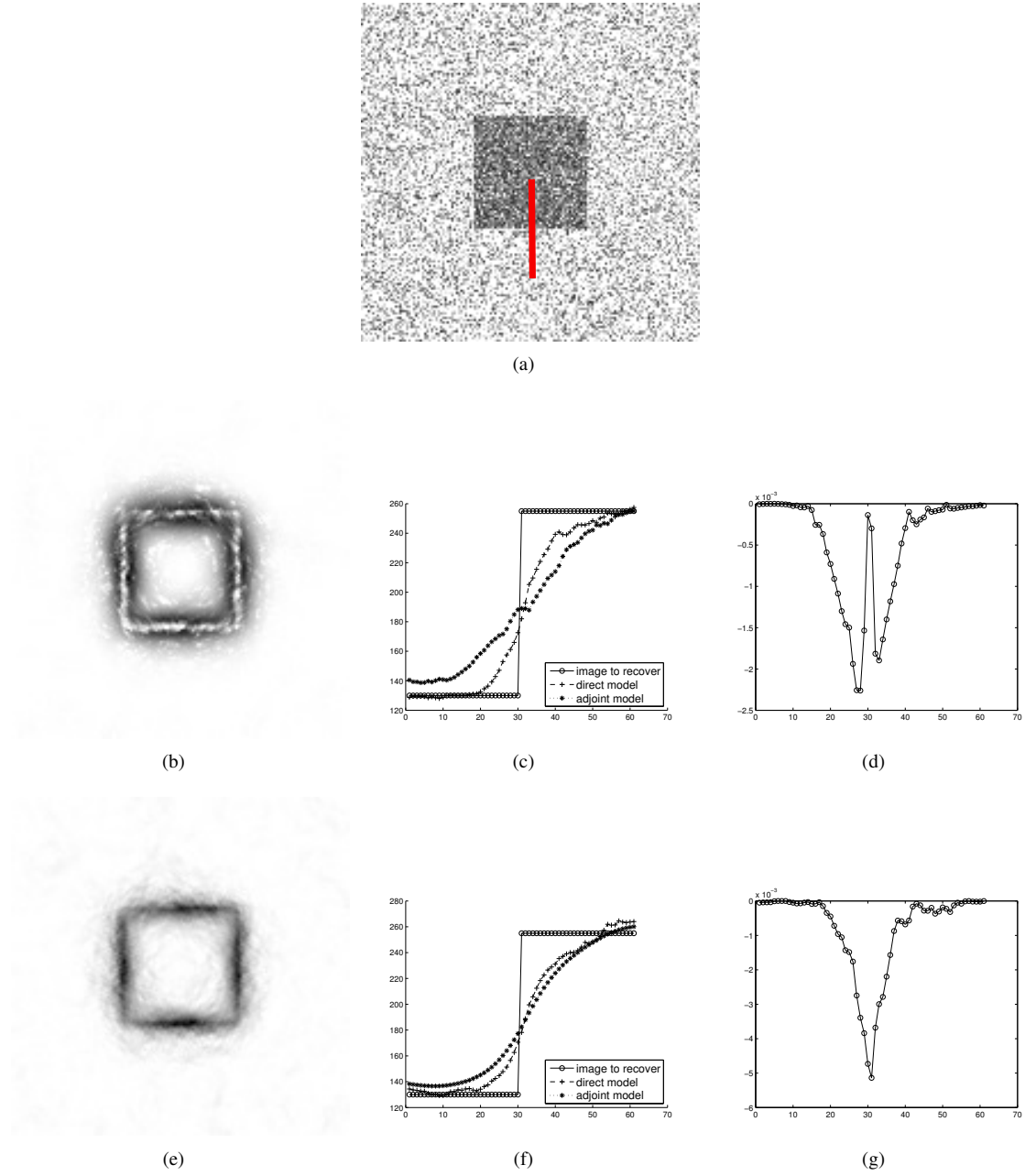


Figure 2: (a) The cut on the speckled image ($L = 6$), (b)-(e) the topological gradients I_{Lap}^c (15) ($\gamma = 30$), (c)-(f) a transverse cut displaying the image to recover, the direct and the adjoint models, (d)-(e) a transverse cut of I_{Lap}^c . (b)-(c)-(d) are associated to $\tilde{J}(\Omega, u)$ and (e)-(f)-(g) to $\tilde{J}_2(\Omega, u)$

The result given in Fig. 3 for a real SAR image is similar to the one of Fig. 1. Here we see that I_{Lap}^b and I_{Lap}^c can be used for different objectives: particularly on small isotropic structures we see that I_{Lap}^b detects the entire object while I_{Lap}^c and the other indicators detect its edges. Let us notice that I_{Lap}^c detects only edges while the Canny edge detector is also sensitive to texture.

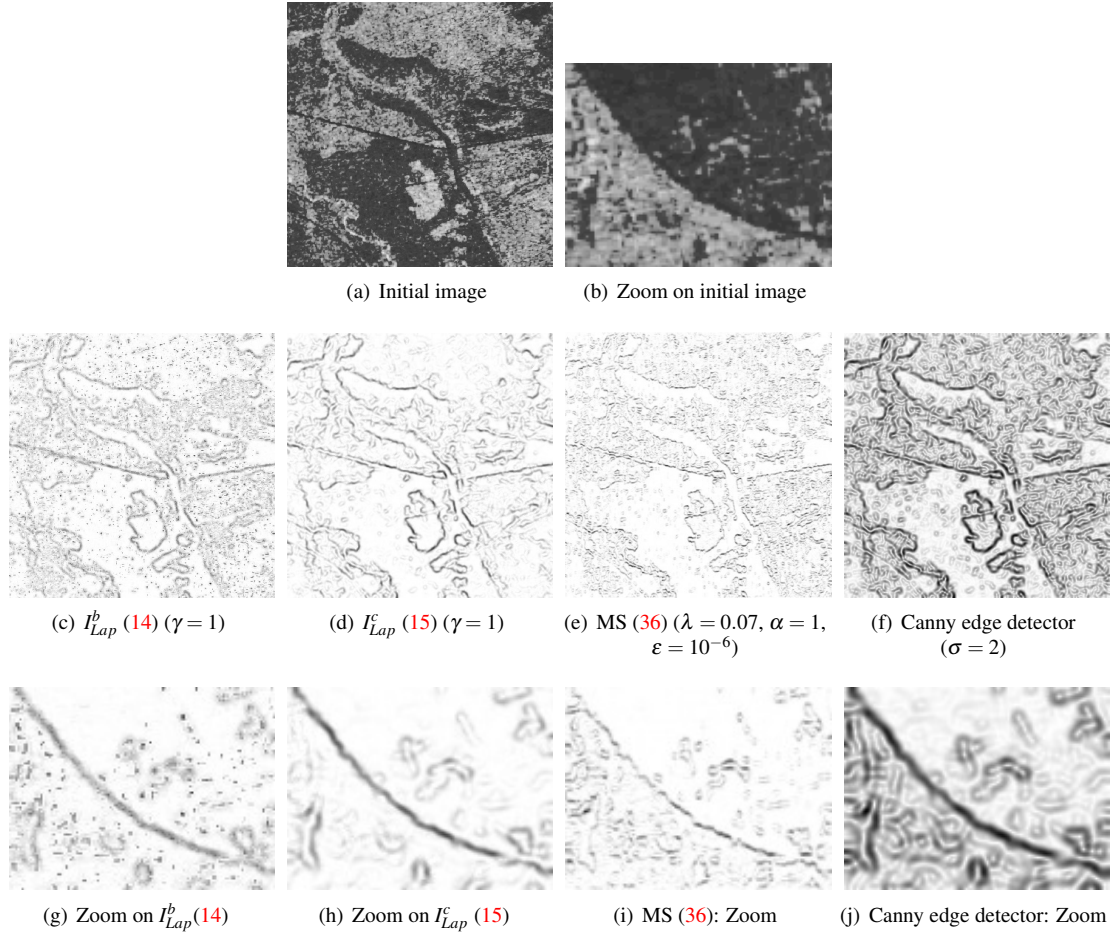


Figure 3: Comparison of (14) and (15) with the MS edge detection (36) and the Canny edge detector for a real SAR image.

Fig. 4 and Fig. 6 compare the restoration performed by (32), (36) and (37) respectively on a real SAR image and on a synthetic speckled image. Restoration given by the MS degrades contours while (32) and the TV model (37) are nearly equivalent. However, on Fig. 6, we can notice that the restoration performed by (32) is better than the TV one and computation times are equivalent (see section 8.5).

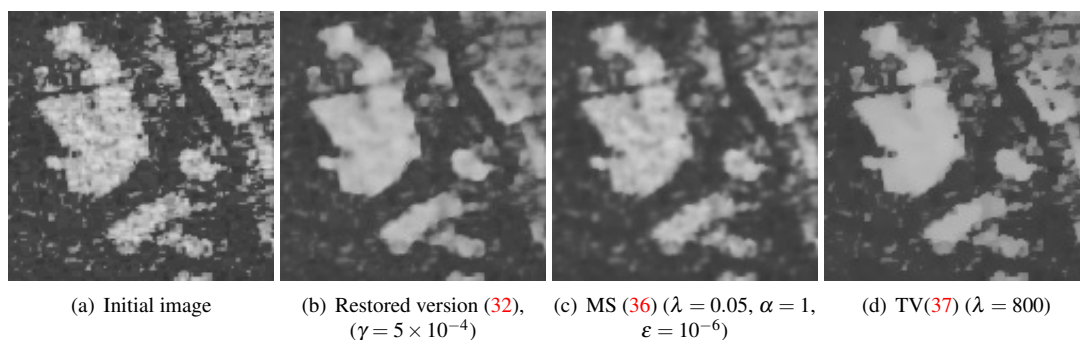


Figure 4: Comparison of the restored versions (32), (36) and (37) for a real SAR image (Zoom on Fig. 3-(a)).

On Fig. 5 we compare $I_{Lap}^c, b(x)$ computed with MS (36) and the Canny edge detector for a very noisy synthetic image ($L = 1$ i.e. the worst case for this model). Here I_{Lap}^c gives a quite good result with respect to MS where edges are spread out and the Canny edge detector which detects a lot of noise.

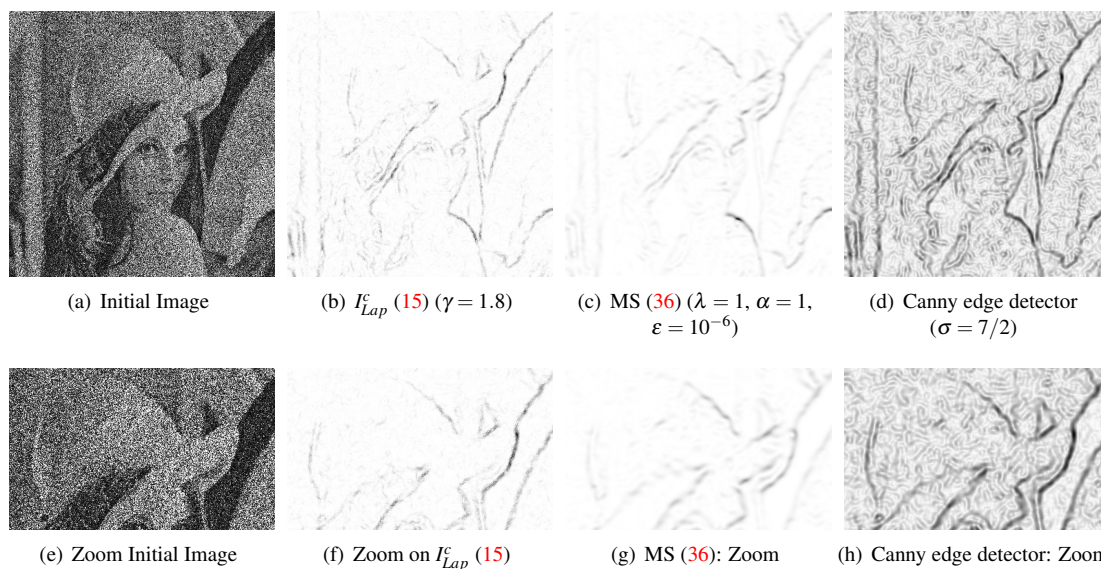


Figure 5: Comparison of the topological gradient (15) with the MS edge detection (36) and the Canny edge detector for a synthetic speckled image ($L = 1$).

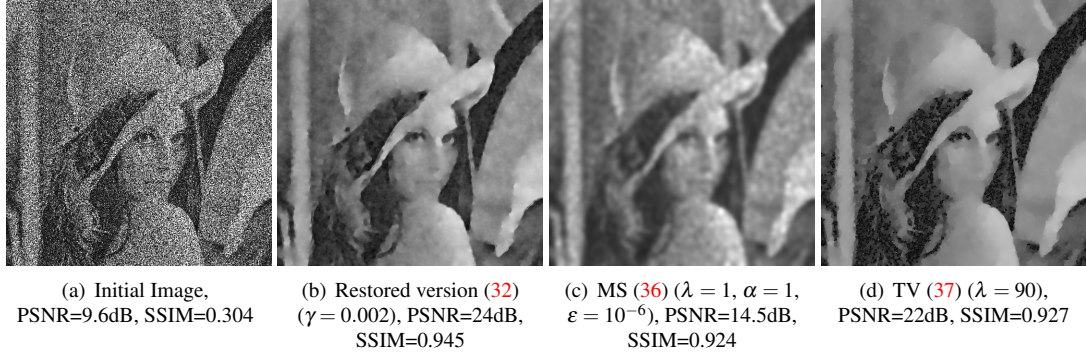


Figure 6: Comparison of restored versions (32), (36) and (37) for a speckled synthetic image ($L = 1$).

Finally Fig. 7 shows the 1D profiles of the image to recover, its noisy version, the restored version (32) and I_{Lap}^c (15) across an edge. The restored version matches very well the image to recover and edges are not degraded except on strong angular point with low contrast where the direction of the diffusion in (32) is not well defined and the topological gradient I_{Lap}^c is low in magnitude. This shows that (32) is a good restoration process.

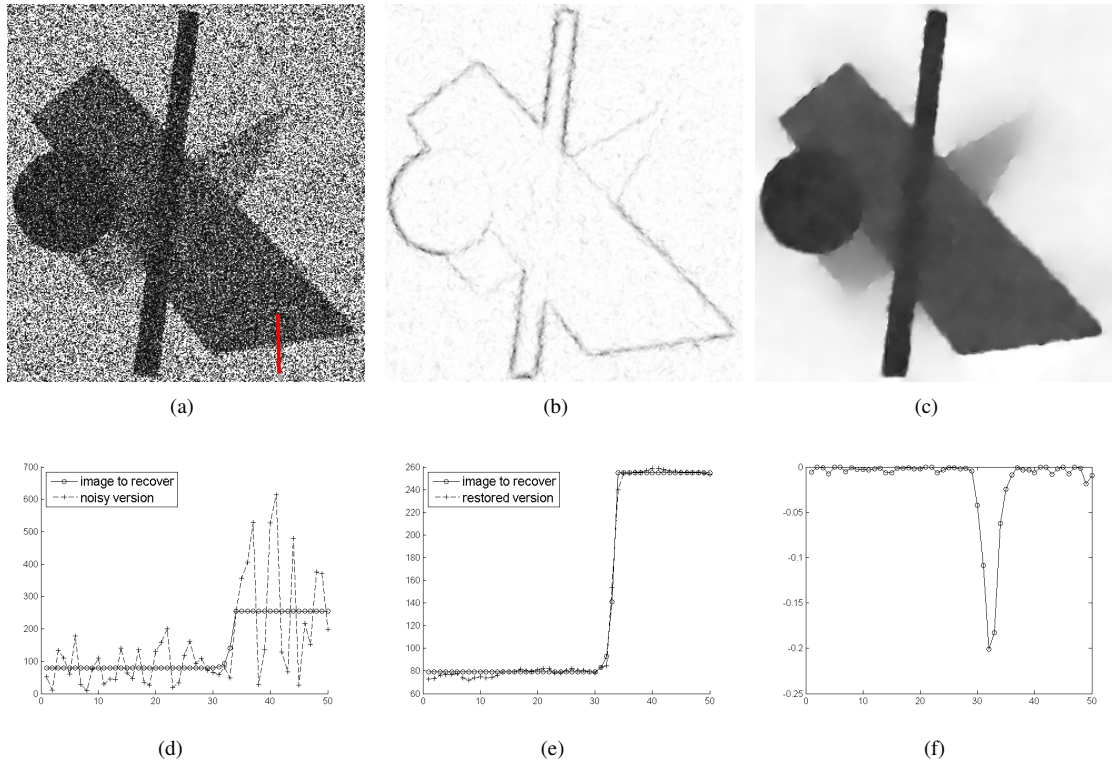


Figure 7: (a)-(d) Image and transverse cut of the speckled image ($L = 1$), (b)-(e) the restored version (32) ($\gamma = 0.01$) and (c)-(f) I_{Lap}^c (15) ($\gamma = 1.8$).

8.4 Numerical results for the Poisson model. Comparisons

In this section we compare the edge detection performed by I_{Lap}^c (31), I_{Lap}^b (21), the MS model (36) and the Canny edge detector. We also compare the restoration computed with (32), the MS and the TV model.

Fig. 8 and Fig. 10 show respectively the edge detection results in the case of a synthetic Poissonian image and of a real confocal image of a rat's neuron. I_{Lap}^c (31) detects edges quite well compared to the MS model. Results performed by the Canny edge detector are similar to those obtained with I_{Lap}^c for small γ while for large γ an edge doubling phenomena still appear. We see that I_{Lap}^b fills small structures (the size of these structures is related to γ as for the speckle case).

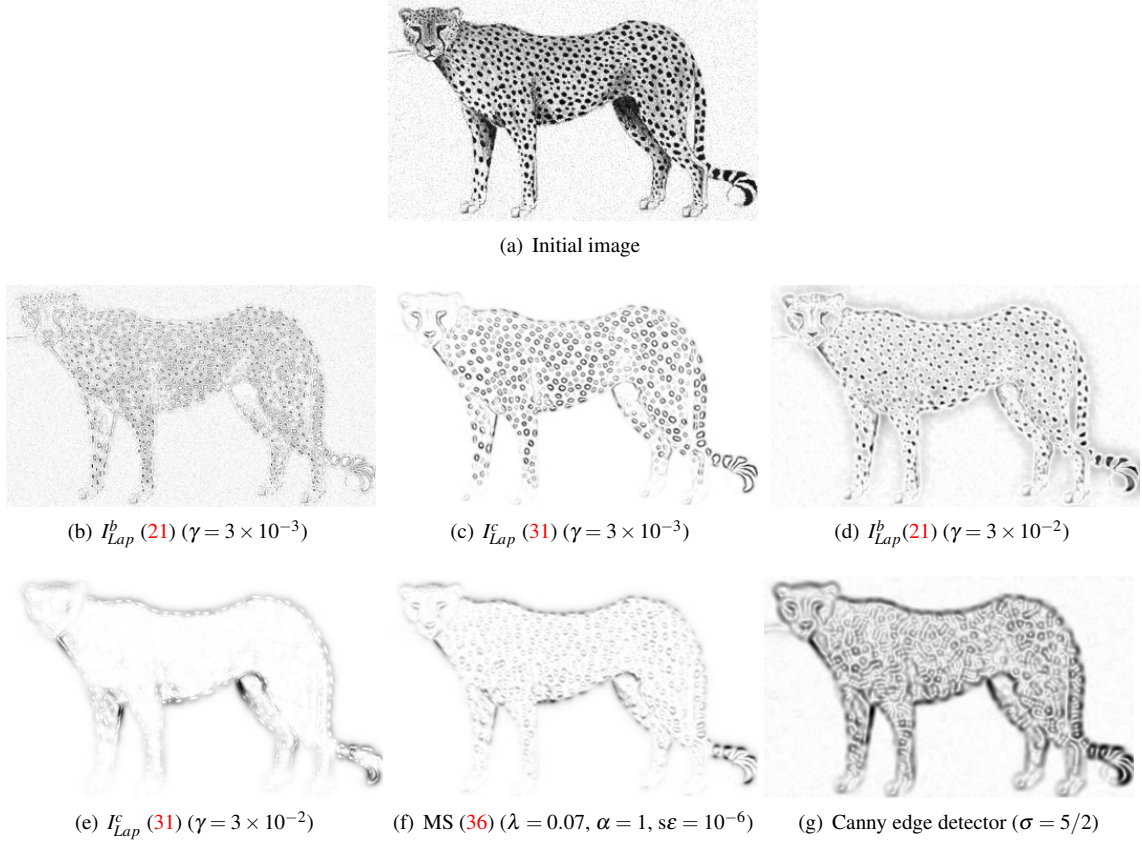
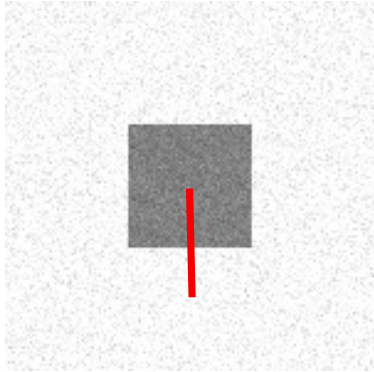


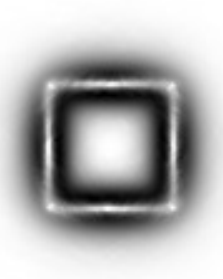
Figure 8: Comparison of (21) and (31) for different values of γ with the MS edge detection (36) and the Canny edge detector for a Poissonian image containing mainly isotropic small structures.

Remark 6. We can still do a similar remark as Remark 5 for Fig. 8-(e). Here also we have remarked that the edge doubling can be avoided for Poissonian model by adding in the cost function the term $\sum_{j=1}^{N_0} \psi_j(I_j(Ku))$. Let us recall that the direct and adjoint models given in (19) and (20) are associated to the auxiliary cost function $\tilde{J}(\Omega, u) = -\sum_{j=1}^{N_0} \int_{\Omega} \psi'_j(I_j(Ku)) I_j(Ku)$. Fig. 9 shows profiles of the direct and adjoint models and I_{Lap}^c (31) associated to $\tilde{J}(\Omega, u)$ and to $\tilde{J}_2(\Omega, u) = \tilde{J}(\Omega, u) + \sum_{j=1}^{N_0} \psi_j(I_j(Ku))$.

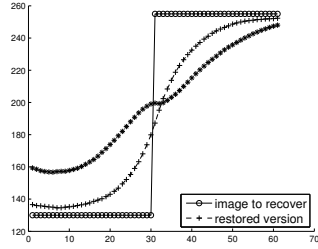
Fig. 12 compares I_{Lap}^c (31) with $b(x)$ performed by the MS model (36) and the Canny edge detector, for a Poissonian image blurred by a Gaussian convolution. Similar results are obtained from the MS model and I_{Lap}^c while edges detected by the Canny edge detector are more spread out (if we decrease the scale parameter σ texture is detected significantly). Fig. 11 and Fig. 13 display the restoration computed by (32), (36) and (37) on respectively a real confocal image and a synthetic Poissonian image blurred by Gaussian convolution. We notice that (32) and (37) restore very well the image preserving edges unlike to the MS model (36) which degrades contours and which does not annihilate the blur effect.



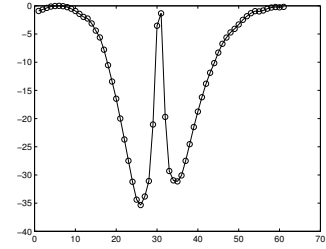
(a)



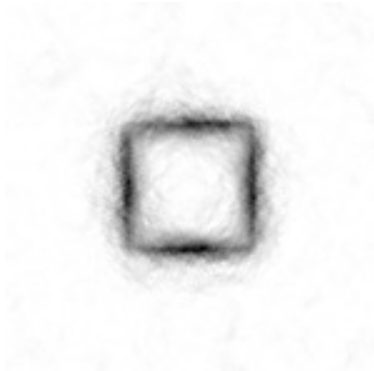
(b)



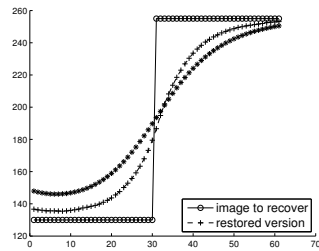
(c)



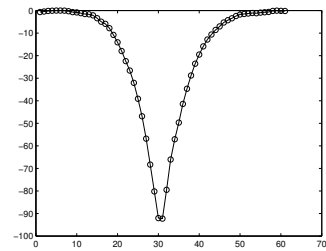
(d)



(e)



(f)



(g)

Figure 9: (a) The cut on the Poissonian image, (b)-(e) the topological gradient I_{Lap}^c (31) ($\gamma = 3 \times 10^{-1}$), (c)-(f) a transverse cut displaying the image to recover, the direct and the adjoint models, (d)-(g) a transverse cut of I_{Lap}^c . (b)-(c)-(d) are associated to $\tilde{J}(\Omega, u)$ and (e)-(f)-(g) to $\tilde{J}_2(\Omega, u)$

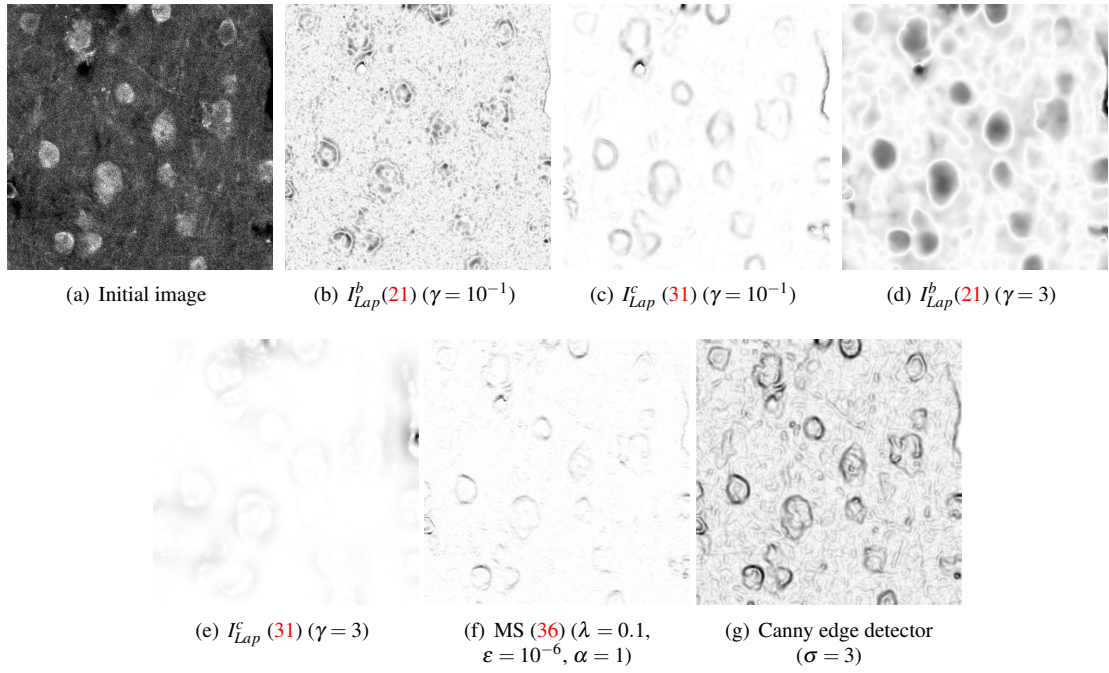


Figure 10: Comparison of (21) and (31) for different values of γ with the MS edge detection (36) and the Canny edge detector for a Poissonian real image containing rat's neurons.

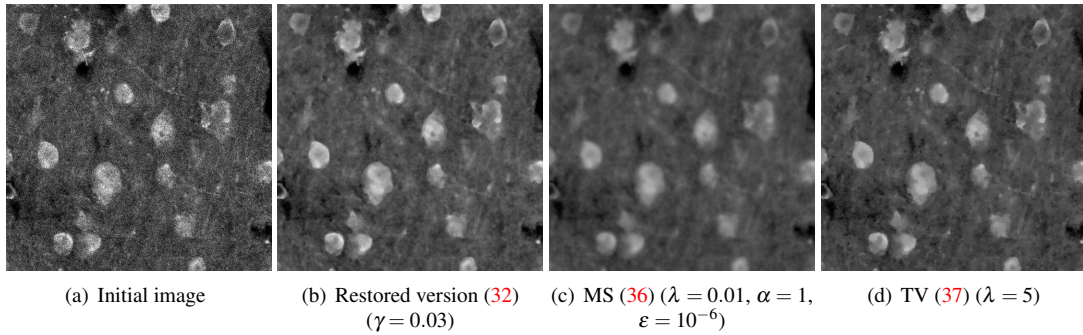


Figure 11: Comparison of the restored versions (32), (36) and (37) for a real Poissonian image of rat's neurons.

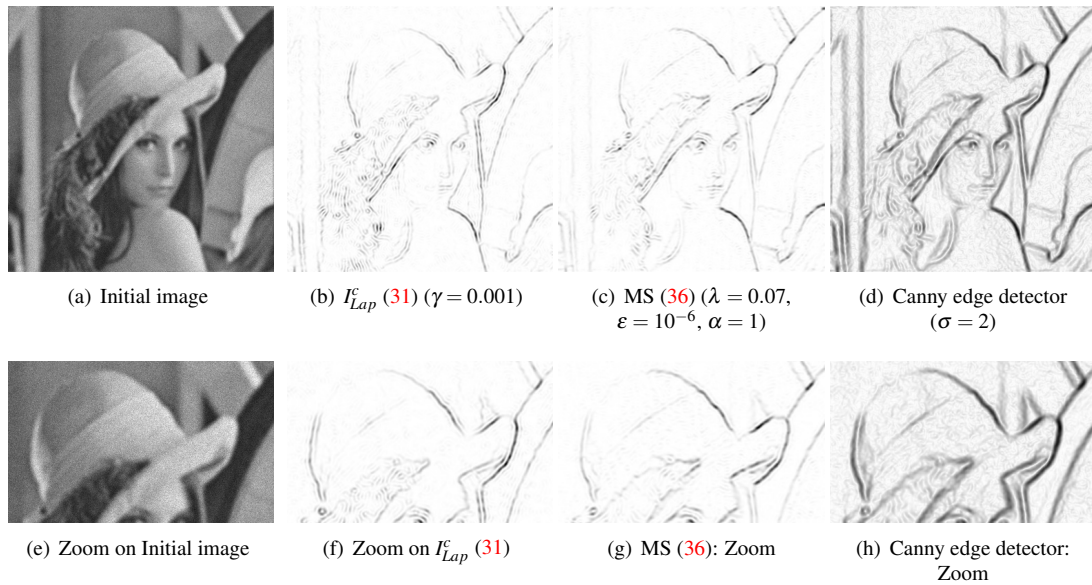


Figure 12: Comparison of I_{Lap}^c (31) with the MS edge detection (36) and the Canny edge detector on a synthetic Poissonian image blurred by a Gaussian convolution of scale $\sigma = 3$.



Figure 13: Comparison of the restored versions for a Poissonian image blurred by a Gaussian convolution of scale $\sigma = 3$.

Finally, Fig. 14 shows the 1D profiles of the image to recover, its degraded versions (blurred, blurred + Poissonian process), the restored version (32) and I_{Lap}^c (31) across an edge. We see that (32) allows to recover the initial image and that I_{Lap}^c detects very well the edge.

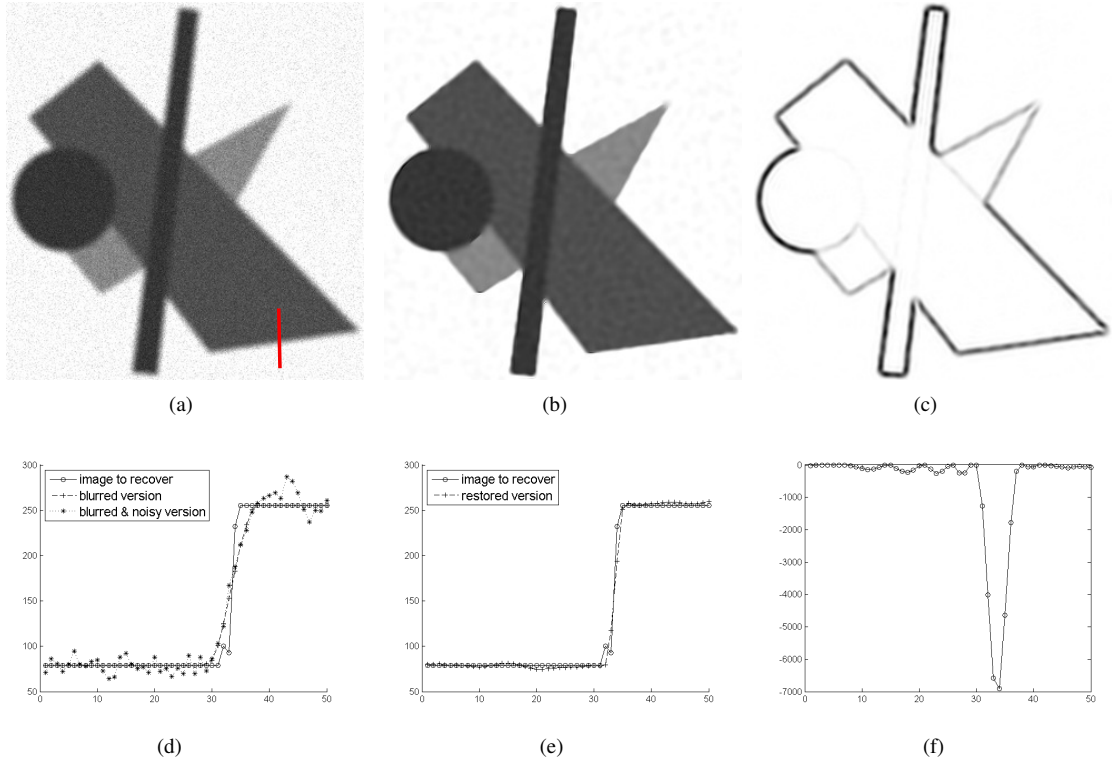


Figure 14: (a)-(d) Image and transverse cut of the Gaussian blurred ($\sigma = 3$) Poissonian image, (b)-(e) the restored version (32) ($\gamma = 0.005$) and (c)-(f) I_{Lap}^c (31) ($\gamma = 0.001$).

8.5 Computational time comparisons for the three methods

On Fig. 15 are compared the three methods for $K = I$ (no blur): Mumford-Shah (MS), TV and the topological gradient method (TG). The experiments are performed on a computer equipped with a processor Intel Core 1.9 GHz and all algorithms are implemented in Matlab. The computation time for the Canny edge detector is not displayed because it just consists in a convolution which is very fast and so it would be very close to the y -axis compared to other methods.

For Poisson and speckle models, the computation of the topological gradient still remains the fastest but the restoration step performed by (32) takes approximately the same time as for a restoration given by a TV model. Let us notice that the TV model is implemented by using an iterative algorithm (explicit schema with fixed step length with at maximum 1000 iterations) and that the Mumford-Shah model solution is computed by minimizing the approximate functional alternatively with respect to u and b . The minimization with respect to u (at b fixed) is made by using Algorithm 2 and we perform 15 iterations. Finally let us precise that we present on Fig. 15 the computation time only for the Poissonian model because similar results are obtained from the speckle one.

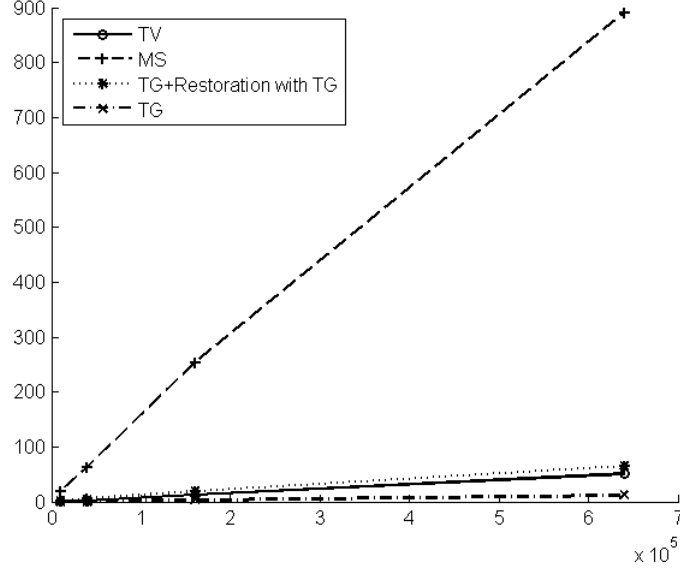


Figure 15: Comparisons of the computational time (in sec.) of the three methods of restoration in function of the number of pixels in the Poissonian case

9 Appendices

In these appendices we give the asymptotic expansion of the differences $u_\varepsilon - u_0$ and $v_\varepsilon - v_0$ for the non linear problems (Poisson and Speckle-log models). Some proofs are similar to the linear case and so we will refer the reader to [5]. To establish these asymptotic expansions we need the following exterior problem

$$(\mathcal{P}_{ext}) \begin{cases} \Delta P = 0 \text{ in } \mathbb{R}^2 \setminus \bar{B} \\ \partial_n P = g \text{ on } \partial B \\ P \rightarrow 0 \text{ at } \infty \end{cases} \quad (38)$$

where $g \in H^{-1/2}(\partial B)$ and $\int_{\partial B} g d\sigma = 0$. For the computation of the topological gradient we will use the two following lemma. We omit the proofs and we refer the reader to [22] for more details

Lemma 9.1. *The solution of (38) expresses as a single layer potential:*

$$P(x) = \int_{\partial B} \lambda(y) E(x-y) d\sigma$$

with $E(x) = -\frac{1}{2\pi} \log(|x|)$ is the fundamental solution of the Laplace operator and $\lambda(y) = -2g(y)$. Denoting by l^P the solution of

$$\begin{cases} \Delta l^P = 0 \text{ in } B \\ \partial_n l^P = 0 \text{ on } \partial B \end{cases}$$

we have the jump relations through ∂B

$$\begin{aligned} P - l^P &= 0 \\ \partial_n P - \partial_n l^P &= -\lambda \end{aligned}$$

and l^P expresses as $l^P(x) = \int_{\partial B} \lambda(y) E(x-y) d\sigma$.

The following asymptotic estimations holds.

Lemma 9.2. *Let P the solution of (38), then:*

$$\begin{aligned} |P(x)| &\leq \frac{C}{|x|}, & |\nabla P(x)| &\leq \frac{C}{|x|^2} \\ \left\| P\left(\frac{x}{\varepsilon}\right) \right\|_{0,\Omega_\varepsilon} &= O\left(\sqrt{-\log(\varepsilon)}\right), & \left\| \nabla P\left(\frac{x}{\varepsilon}\right) \right\|_{0,\Omega_\varepsilon} &= O(\varepsilon) \end{aligned}$$

9.1 Appendix A

In this appendix we perform the asymptotic expansion of u_ε (19) in $H^1(\Omega_\varepsilon)$ -norm when $\varepsilon \rightarrow 0$. We assume along this appendix that $x_0 = 0$.

Lemma 9.3. *Let $X_\varepsilon = u_\varepsilon - u_0$ where u_ε and u_0 are respectively given by (19) for $\varepsilon > 0$ and $\varepsilon = 0$, then we have:*

$$X_\varepsilon = \varepsilon P\left(\frac{x}{\varepsilon}\right) + e_\varepsilon$$

where P is defined by (38) with $g = -\nabla u_0(0) \cdot \mathbf{n}$ and where $\|e_\varepsilon\|_{1,\Omega_\varepsilon} = O(\varepsilon^2)$. Moreover we have the estimation:

$$\|X_\varepsilon\|_{0,\Omega_\varepsilon} = O(\varepsilon^2 \sqrt{-\log(\varepsilon)})$$

Proof. First, let us write the Euler equations checked by X_ε . By subtracting equations (19) for $\varepsilon > 0$ and for $\varepsilon = 0$, we get for $j \in \{1, \dots, N_0\}$:

$$(\mathcal{X}_\varepsilon) \begin{cases} -\Delta X_\varepsilon + \psi'_j \left(\int_{R_j^\varepsilon} K u_\varepsilon \right) - \psi'_j \left(\int_{R_j} K u_0 \right) = 0 \text{ in } R_j^\varepsilon, j \in \{1, \dots, N_0\} \\ \partial_n X_\varepsilon = -\partial_n u_0, \text{ on } \partial B_\varepsilon \\ \partial_n X_\varepsilon = 0, \text{ on } \Gamma \end{cases} \quad (39)$$

Then, by a Taylor expansion, there exists $\xi_\varepsilon^j \in]\int_{R_j} K u_0, \int_{R_j^\varepsilon} K u_\varepsilon[$ such that

$$\psi'_j \left(\int_{R_j^\varepsilon} K u_\varepsilon \right) - \psi'_j \left(\int_{R_j} K u_0 \right) = \psi''_j(\xi_\varepsilon^j) \left(\int_{R_j^\varepsilon} K u_\varepsilon - \int_{R_j} K u_0 \right)$$

From Proposition 2, it is straightforward that $0 < \alpha \leq \xi_\varepsilon^j \leq \beta$ where $\alpha = \frac{\min_i f_i}{N}$ and $\beta = \sum_i f_i$. $(\mathcal{X}_\varepsilon)$ rewrites for $j \in \{1, \dots, N_0\}$ as

$$(\mathcal{X}_\varepsilon) \begin{cases} -\Delta X_\varepsilon + \psi''_j(\xi_\varepsilon^j) \int_{R_j^\varepsilon} K X_\varepsilon = \int_{R_j \setminus \overline{R_j^\varepsilon}} K u_0 \text{ in } R_j^\varepsilon \\ \partial_n X_\varepsilon = -\partial_n u_0, \text{ on } \partial B_\varepsilon \\ \partial_n X_\varepsilon = 0, \text{ on } \Gamma \end{cases}$$

with $\int_{R_j \setminus \overline{R_j^\varepsilon}} K u_0 = \delta_{j_0}(j) \int_{B_\varepsilon} K u_0$, where δ is the Dirac function. Let $e_\varepsilon = X_\varepsilon - \varepsilon P\left(\frac{x}{\varepsilon}\right)$ where P is defined by

By taking as test function $v = e_\varepsilon^3$ in (41), we deduce the following estimations:

$$\begin{aligned}
& \int_{\Omega_\varepsilon} |\nabla e_\varepsilon^3|^2 + C \sum_{j=1}^{N_0} \left(\int_{R_j^\varepsilon} K e_\varepsilon^3 \right)^2 \\
& \leq \sum_{j=1}^{N_0} |\mathcal{F}_\varepsilon^j| \left| \int_{R_j^\varepsilon} K e_\varepsilon^3 \right| + |\psi_j''(\xi_\varepsilon^j)| \int_{R_j^\varepsilon} (|K e_\varepsilon^1| + |K e_\varepsilon^2|) \left| \int_{R_j^\varepsilon} K e_\varepsilon^3 \right| \\
& \leq C \left(\varepsilon^2 + \|e_\varepsilon^1\|_{L^2(\Omega_\varepsilon)/\mathbb{R}} + \|e_\varepsilon^2\|_{L^2(\Omega_\varepsilon)/\mathbb{R}} \right) \sum_{j=1}^{N_0} \left| \int_{R_j^\varepsilon} K e_\varepsilon^3 \right| \\
& \leq C \varepsilon^2 \sum_{j=1}^{N_0} \left| \int_{R_j^\varepsilon} K e_\varepsilon^3 \right|
\end{aligned}$$

Then, thanks to the following inequality which stands for any sequence of real numbers $(a_i)_i$

$$\left(\sum_{i \in \{1, \dots, N_0\}} |a_i| \right)^2 \leq N_0 \sum_{j=1}^{N_0} |a_j|^2$$

and the positiveness of $\int_{\Omega_\varepsilon} |\nabla e_\varepsilon^3|^2$, we obtain

$$\sum_{j=1}^{N_0} \left| \int_{R_j^\varepsilon} K e_\varepsilon^3 \right| \leq C \varepsilon^2$$

and then $\|e_\varepsilon^3\|_{1, \Omega_\varepsilon} \leq C \varepsilon^2$. By splitting e_ε^3 into the sum $e_\varepsilon^3 = \left(e_\varepsilon^3 - \frac{1}{|\Omega|} \int_{\Omega_\varepsilon} e_\varepsilon^3 \right) + \frac{1}{|\Omega|} \int_{\Omega_\varepsilon} e_\varepsilon^3$ and using Poincaré-Wirtinger inequality and the fact that $K \mathbb{1} \neq 0$ (as in Proposition 2) we get $\|e_\varepsilon^3\|_{1, \Omega_\varepsilon} \leq C \varepsilon^2$.

From the inequality $\|e_\varepsilon\|_{1, \Omega_\varepsilon} \leq \|e_\varepsilon^1\|_{H^1(\Omega_\varepsilon)/\mathbb{R}} + \|e_\varepsilon^2\|_{H^1(\Omega_\varepsilon)/\mathbb{R}} + \|e_\varepsilon^3\|_{1, \Omega_\varepsilon}$, we obtain the estimation. For the $L^2(\Omega_\varepsilon)$ -norm estimation of X_ε , it suffices to take the $L^2(\Omega_\varepsilon)$ -norm of its asymptotic expansion and to use the first point of Lemma 9.3 and Lemma 9.2. \square

Lemma 9.4. *Let $w_\varepsilon = v_\varepsilon - v_0$ where v_ε and v_0 are given by (26) for $\varepsilon > 0$ and $\varepsilon = 0$, then we have:*

$$w_\varepsilon = \varepsilon P \left(\frac{x}{\varepsilon} \right) + r_\varepsilon$$

where P is defined by (38) with $g = -\nabla v_0(0) \cdot n$, and where $\|r_\varepsilon\|_{1, \Omega_\varepsilon} = O(\varepsilon^2 \sqrt{-\log(\varepsilon)})$. Moreover we have:

$$\|w_\varepsilon\|_{0, \Omega_\varepsilon} = O(\varepsilon^2 \sqrt{-\log(\varepsilon)}), \quad \|w_\varepsilon\|_{1, \Omega_\varepsilon} = O(\varepsilon)$$

Proof. By subtracting equations (20) for $\varepsilon > 0$ and for $\varepsilon = 0$, the Euler equations associated to w_ε are:

$$(\mathcal{W}_\varepsilon) \left\{ \begin{array}{l} -\Delta w_\varepsilon + \psi_j''(I_j(u_0)) \int_{R_j^\varepsilon} K w_\varepsilon = 0 \text{ in } R_j \text{ with } j \neq j_0 \\ -\Delta w_\varepsilon + \psi_{j_0}''(I_{j_0}(Ku_0)) \int_{R_{j_0}^\varepsilon} K w_\varepsilon = \psi_{j_0}''(I_{j_0}(Ku_0)) \int_{B_\varepsilon} K v_0 = O(\varepsilon^2) \text{ in } R_{j_0}^\varepsilon \\ \partial_n w_\varepsilon = -\partial_n v_0 \text{ on } \partial B_\varepsilon \\ \partial_n w_\varepsilon = 0 \text{ on } \Gamma \end{array} \right. \quad (42)$$

This problem is linear and from Proposition 2 we have:

$$\frac{\min_{j \in \{1, \dots, N_0\}} f_j}{\beta^2} \leq \psi_j''(I_j(u_0)) = \frac{f_j}{I_j(u_0)^2} \leq \frac{\max_{j \in \{1, \dots, N_0\}} f_j}{\alpha^2}$$

Then the topological expansion of w_ε can be deduced from the proof of Lemma 9.3 or from the linear case with constant coefficient [5]. See also Nedelec [35] for details on the analysis.

The two last estimations are straightforward by using the topological expansion of w_ε and Lemma 9.2. \square

References

- [1] L. Ambrosio and V.M. Tortorelli. Approximation of functionals depending on jumps by elliptical functionals via Gamma-convergence. *Communications on Pure and Applied Mathematics*, XLIII:999–1036, 1990.
- [2] S. Amstutz. Topological sensitivity analysis for some nonlinear PDE system. *J. Math. Pures Appl.*, 2006.
- [3] S. Amstutz. The topological asymptotic for the Navier-Stokes equations. *ESAIM: Control, Optimisation and Calculus of Variations*, 11(3):401–425, 3 2010.
- [4] S. Amstutz and J. Fehrenbach. Edge detection using topological gradients: a scale-space approach (preprint). July 2014.
- [5] S. Amstutz, I. Horchani, and M. Masmoudi. Crack detection by the topological gradient method. *Control and Cybernetics*, 34(1):81–101, 2005.
- [6] G. Aubert and J-F. Aujol. A variational approach to removing multiplicative noise. *SIAM Journal of Applied Mathematics*, 68(4):925–946, 2008.
- [7] G. Aubert and A. Drogoul. Topological gradient for a fourth order operator used in image analysis (To appear COCV).
- [8] G. Aubert and A. Drogoul. Topological gradient for fourth order pde and application to the detection of fine structures in 2d images. *C. R. Math. Acad. Sci. Paris*, 352:609–613, 2014.
- [9] G. Aubert and P. Kornprobst. *Mathematical Problems in Image Processing: Partial Differential Equations and the Calculus of Variations (second edition)*, volume 147 of *Applied Mathematical Sciences*. Springer-Verlag, 2006.
- [10] D. Auroux. From restoration by topological gradient to medical image segmentation via an asymptotic expansion. *Math. Comput. Model.*, 49(11-12):2191–2205, 2009.
- [11] D. Auroux and M. Masmoudi. A one-shot inpainting algorithm based on the topological asymptotic analysis. *Computational & Applied Mathematics*, 25:251 – 267, 2006.
- [12] D. Auroux and M. Masmoudi. Image processing by topological asymptotic expansion. *Journal of Mathematical Imaging and Vision*, 33(2):122–134, 2009.
- [13] D. Auroux, M. Masmoudi, and L. Jaafar Belaid. *Image restoration and classification by topological asymptotic expansion*, pages 23–42. *Variational Formulations in Mechanics: Theory and Applications*, E. Taroco, E.A. de Souza Neto and A.A. Novotny (Eds). CIMNE, Barcelona, Spain, 2007.

- [14] H. Ayasso and A. Mohammad-Djafari. Joint image restoration and segmentation using Gauss-Markov-Potts prior models and variational Bayesian computation. In *16 th IEEE International Conference on Image Processing (ICIP)*, pages 1297–1300, 2009.
- [15] L. Jaafar Belaid, M. Jaoua, M. Masmoudi, and L. Siala. Image restoration and edge detection by topological asymptotic expansion. *C. R. Acad. Sci. Paris*, 342(5):313 – 318, 2006.
- [16] L. Jaafar Belaid, M. Jaoua, M. Masmoudi, and L. Siala. Application of the topological gradient to image restoration and edge detection. *Engineering Analysis with Boundary Elements*, 32(11):891 – 899, 2008.
- [17] S. Ben Hadj, L. Blanc Féraud, and G. Aubert. Space Variant Blind Image Restoration. *SIAM Journal on Imaging Sciences*, 7(4):49, 2014.
- [18] S. Bonettini, R. Zanella, and L. Zanni. A scaled gradient projection method for constrained image deblurring. *Inverse Problems*, 25(1):015002, 2009.
- [19] T. Chan and J. Shen. *Image Processing And Analysis : Variational, Pde, Wavelet, and Stochastic*.
- [20] N. Dey, L. Blanc-Féraud, C. Zimmer, P. Roux, Z. Kam, J-C. Olivo-Marin, and J. Zerubia. 3D Microscopy Deconvolution using Richardson-Lucy Algorithm with Total Variation Regularization. Rapport de recherche RR-5272, INRIA, 2004.
- [21] A. Drogoul. Numerical analysis of the topological gradient method for fourth order models and applications to the detection of fine structures in 2D imaging (To appear SIAM J. Imaging Sciences).
- [22] A. Drogoul. Topological gradient method applied to the detection of edges and fine structures in imaging. *Phd Thesis University of Nice Sophia Antipolis*, 2014.
- [23] S. Geman and D. Geman. Stochastic Relaxation, Gibbs Distributions, and the Bayesian Restoration of Images. *IEEE Transactions on Pattern Analysis and Machine Intelligence*, 6(6):721–741, 1984.
- [24] T. Hebert and R. Leahy. A generalized EM algorithm for 3D Bayesian reconstruction from Poisson data using Gibbs prior. *IEEE Trans. Medical imaging*, 8(2):194–202, 1989.
- [25] F.M. Henderson, A.J. Lewis, and R.A. Ryerson, editors. *Principles and applications of imaging radar*. Manual of remote sensing. Wiley, New York, 1998. Manual of remote sensing edited by Robert A. Ryerson.
- [26] M. Hintermüller. Fast-set based algorithms using shape and topological sensitivity information. *Control and Cybernetics*, 34(1):305 – 324, 2005.
- [27] M. Iguernane, S. A. Nazarov, J-R. Roche, J. Sokolowski, and K. Szulc. Topological derivatives for semilinear elliptic equations. *Applied Mathematics and Computer Science*, 19(2):191–205, 2009.
- [28] K. Krissian, R. Kikinis, C-F. Westin, and K.G. Vosburgh. Speckle-constrained filtering of ultrasound images. In *CVPR (2)*, pages 547–552. IEEE Computer Society, 2005.
- [29] S. Larnier and J. Fehrenbach. Edge detection and image restoration with anisotropic topological gradient. In *Proceedings ICASSP, International Conference on Acoustic Speech and Signal Processing*, pages 1362–1365, 2010.
- [30] S. Larnier, J. Fehrenbach, and M. Masmoudi. The topological gradient method : from optimal design to image processing. *Milan Journal of Mathematics*, 80(2):411–441, 2012.

- [31] I. Larrabide, A.A. Novotny, R.A. Feijo, and E. Taroco. A medical image enhancement algorithms based on topological derivative and anisotropic diffusion. In *Proceedings of the XXVI Iberian Latin-American Congress on Computational methods in Engineering*, 2005.
- [32] S. Mallat. *A Wavelet Tour of Signal Processing*. Academic Press, 1998.
- [33] M. Masmoudi. The topological asymptotic. In *Computational Methods for Control Applications*, volume 16 of *GAKUTO Internat. Ser. Math. Appl., Tokyo, Japan*, 2001.
- [34] D. Mumford and J. Shah. Optimal approximations by piecewise smooth functions and associated variational problems. *Communications on Pure and Applied Mathematics*, 42(5):577–685, 1989.
- [35] J-C. Nédélec. *Acoustic and electromagnetic equations : integral representations for harmonic problems*. Applied mathematical sciences. Springer, New York, 2001.
- [36] J. Pawley. *Handbook of Biological Confocal Microscopy*. Springer, Berlin, 2006.
- [37] A. Sawatzky, D. Tenbrinck, X. Jiang, and M. Burger. A variational framework for region-based segmentation incorporating physical noise models. *Journal of Mathematical Imaging and Vision*, 47(3):179–209, 2013.
- [38] J. Serra. *Image Analysis and Mathematical Morphology*. Academic Press, Inc., Orlando, FL, USA, 1983.
- [39] J. Sokolowski and A. Zochowski. On the topological derivative in shape optimization. *SIAM J. Control Optim.*, 37(4):1251–1272, April 1999.
- [40] M. Tur, K. C. Chin, and J. W. Goodman. When is speckle noise multiplicative? *Applied Optics*, 21(7):1157–1159, 1982.
- [41] M.N. Wernick and J.N.(eds) Aarsvold. *Emission tomography: The fundamental of PET and SPECT*. Elsevier, Amsterdam, 2004.